Thesis for the degree of Doctor of Engineering

Turbulent transport in tokamak plasmas: linear-, quasi- and non-linear simulations

Emil Fransson

CHALMERS
UNIVERSITY OF TECHNOLOGY

Department of Space, Earth and Environment
Division of Astronomy and Plasma Physics
Chalmers University of Technology
Gothenburg, Sweden 2023

Turbulent transport in tokamak plasmas: linear-, quasi- and non-linear simulations

Emil Fransson

Division of Astronomy and Plasma Physics
Department of Space, Earth and Environment
Chalmers University of Technology
SE-412 96 Gothenburg
Telephone +46 31 772 1000

Contact information:
Emil Fransson
Hörsalsvägen 11
Chalmers University of Technology
SE–412 58 Gothenburg, Sweden

Phone: +46 (0)31 772 15 67
Email: emil.fransson@chalmers.se

ISBN: 978-91-7905-839-5
Löpnummer: 5305 i serien Doktorsavhandlingar vid Chalmers tekniska högskola. Ny serie (ISSN0346-718X)

Printed by Chalmers Reproservice
Gothenburg, Sweden 2023

Turbulent transport in tokamak plasmas: linear-, quasi- and non-linear simulations

Emil Fransson
Department of Space Earth and Environment
Chalmers University of Technology

Abstract

An attractive energy source is nuclear fusion with its abundance of fuel, intrinsic safety and limited environmental impact. Although the concept of fusion energy was established in the 1920s, to develop fusion as an energy source has been challenging. The most developed concept for fusion is the tokamak, a torodial shaped chamber where a plasma, a hot ionized gas, is confined with a strong magnetic field. The feasibility and efficiency of the future fusion power plants depend critically on the energy confinement properties of the tokamaks which are mainly determined by micro turbulence. The turbulent transport is driven by different instabilities in the plasma, especially the Ion Temperature Gradient (ITG) mode, Trapped Electron Mode (TEM) and Electron Temperature Gradient (ETG) mode. The work presented in this thesis focuses on a number of key aspects of turbulent transport using advanced numerical modelling tools.

In today's experiments, measurements have shown the plasma's densities to be peaked towards the centre of the plasma. Research into this peaking has uncovered two key mechanisms, a strong particle pinch from the turbulent transport and a particle source from Neutral Beam Injection which is used to heat plasma. In future tokamaks the source will be comparatively smaller, hence it is important to distinguish which of the two provides the dominant contribution. Which is one of the aspects analysed in the thesis.

From basic considerations, the turbulent transport should exhibit so called gyro-Bohm scaling, i.e. the transport should increase with the ionic mass. However, this is not observed experimentally and the discrepancy is called the isotope effect. Several mechanism has been suggested as the cause, such as collisions, ExB shear, β-effects, edge effects and contribution of the ETG mode. A number of JET discharges design to study this isotope effect have been analysed to asses the relative importance of these effects,

Calculation of the turbulent transport can be computationally expensive, therefore reduced quasi-linear models that are computationally less intensive have been developed. These models use linear relations between perturbed quantities combined with a saturation rule for the electrostatic potential to determine the turbulent fluxes. A saturation rule adapted to a quasi-linear model has been developed and validated against non-linear gyro-kinetic simulations which are characterized by a high degree of physics fidelity.

Keywords: Fusion – Plasma physics – Turbulent transport – Gyrofluid – Gyrokinetic

Research contributions

This thesis is based on the work contained in the following papers:

I. F Eriksson, E Fransson, M Oberparleiter, H Nordman1, P Strand, A Salmi, T Tala and JET Contributors
Interpretative and predictive modelling of JET collisionality scans
Plasma Phys. Control. Fusion **61**, 102487 (2019)

II. S. Mordijck, T.L. Rhodes, L. Zeng, A. Salmi, T. Tala, C.C. Petty, G.R. McKee, R. Reksoatmodjo, F. Eriksson, E. Fransson and H. Nordman:
Collisionality driven turbulent particle transport changes in DIII-D H-mode plasmas
Nucl. Fusion **60**, 066019 (2020)

III. E. Fransson, F. Eriksson, M. Oberparleiter, M. Held, S. Mordijck, H. Nordman, A. Salmi, P. Strand, T. Tala and JET contributors:
Comparing particle transport in JET and DIII-D plasmas: gyrokinetic and gyrofluid modelling
Nucl. Fusion **61**, 016015 (2021)

IV. E. Fransson, H. Nordman, P. Strand and JET Contributors
Upgrade and benchmark of quasi-linear transport model EDWM
Physics of Plasmas **29**, 112305 (2022)

V. E. Fransson, L.-G. Eriksson, D.B. King, H. Nordman, P. Strand, E. Viezzer, D. Yadikin and JET Contributors
On the role of the main isotope for the core confinement in JET H-modes
Submitted to Nucl. Fusion

Other research contributions

VI. T. Tala et al including Emil Fransson
Density Peaking in JET - Driven by Fuelling or Transport?
Nucl. Fusion **59**, 126030 (2019)

VII. E. Fransson, F.Eriksson, M.Oberparleiter, M. Held, S. Mordijck, H.Nordman, A. Salmi, P.Strand, T. Tala and JET contributors
Comparison particle transport in JET and DIII-D plasmas: gyrokinetic and gyrofluid modelling
In Proceedings of 62nd Annual Meeting of the APS Division of Plasma Physics (2020)

VIII. E. Militello Asp et al including Emil Fransson
Global JINTRAC Simulations for ITER PFPO Scenario Development
In Proceedings of 28th IAEA Fusion Energy Conference (2021)

IX. O. Sauter et al including Emil Fransson
ITER baseline scenario investigations on TCV and comparison with AUG
In Proceedings of 28th IAEA Fusion Energy Conference (2021)

X. T. Tala et al including Emil Fransson
Comparison of Particle Transport and Confinement Properties between the ICRH and NBI Heated Dimensionless Identity Plasmas on JET
In Proceedings of 28th IAEA Fusion Energy Conference (2021)

XI. A. Gillgren, E. Fransson, D. Yadykin, L. Frassinetti, P. Strand and JET Contributors
Enabling adaptive pedestals in predictive transport simulations using neural networks
Nucl. Fusion **62**, 096006 (2022)

XII. E. Fransson, H. Nordman and P. Strand
Quasi-Linear transport model EDWM: Update and benchmarking
In Proceedings of 48th EPS Conference on Plasma Physics (2022)

XIII. H.-T. Kim et al including Emil Fransson
Validation of DT fusion power prediction capability against 2021 JET DT experiments
To be submitted to Nucl. Fusion

Acknowledgements

Firstly, I would like to thank my supervisor Pär Strand who has been an immense support during my years at Chalmers. Michael Oberparleiter helped me greatly when I started my PhD and I will not forget his kindness. It gives me pleasure to thank Hans Nordman and Lars-Göran Eriksson. Our Friday meetings will be one of the things I will look back on with the most fondness from my PhD-time at Chalmers. I would also like to thank my colleagues at the Plasma Physics group for making it an inspiring and fun workplace. Finally, I would like to thank Noah, August, Algot, Iris och Adeline for just being themselves.

Emil Fransson, Gothenburg, March 2023

Glödet
och
Oan

CONTENTS

CHAPTER 1

INTRODUCTION

The sun has always had a special place in human history, first as a God later as the center of the solar system but always as a source of warmth and energy. To emulate this virtually infinite energy source have been a dream for humans since the 1950s when research into nuclear fusion took off in earnest.

1.1 Fusion

The energy from the sun is produced by nuclear fusion which is the process of two lighter elements fusing together into a heavier one. This process yields excess energy for all nuclei where the product is lighter than iron, due to the binding energy of the nuclei. The binding energy per nuclei is displayed in Figure (1.1), and the highest binding energy is for iron, Fe.

In a similar fashion, if we split an element heavier than iron we would release energy, this process is called fission. Fission is usually done with a neutron as the instigator. A major challenge with fusion is that both nuclei are positively charged and the nuclei need large kinetic energy to overcome the Coulomb repul-

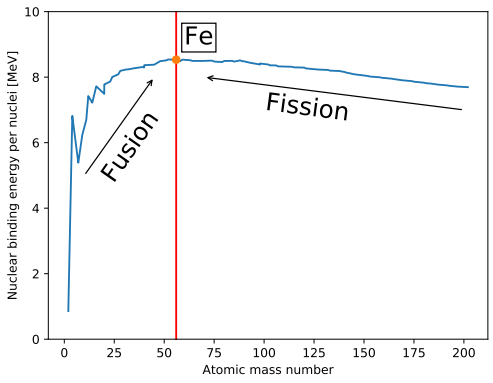

Figure 1.1: *Binding energy*

sion. To achieve nuclear fusion energy here on earth the reacting nuclei need to be contained for long enough time and at high enough temperature. This is achieved in the stars by the means of gravitation, which is obviously not an option on earth. The fusion process in the stars begins with the fusion of two protons. This process is however not suitable for a fusion power plant on earth due to the low cross section of the reaction. There are a number of processes which are more promising, specifically the ones between two Deuterium nuclei and Deuterium and Tritium.

$$D + D \rightarrow He^3\ (0.82\ MeV) + n\ (2.45\ MeV) \tag{1.1a}$$
$$D + D \rightarrow T\ (1.01\ MeV) + H\ (3.02\ MeV) \tag{1.1b}$$
$$D + T \rightarrow He^4\ (3.52\ MeV) + n\ (14.06\ MeV) \tag{1.1c}$$

An important thing to notice about these processes is that they do not create any radioactive waste product as He^4 is a stable isotope. The reaction rate of these processes are governed by their cross sections which are shown in Figure (1.2). We can notice that the cross section is much higher for D+T than for D+D, therefore the former process is the one that the scientific community is primarily perusing. However, this process has some drawbacks as Tritium is an unstable hydrogen isotope and has a half-life of 12.3 years. As a result, the isotope is extremely rare in nature and hard to store. A solution to this is for the fusion power plants to breed their own Tritium. This can be done by bombarding Lithium with neutrons created in Deuterium - Tritium reactions, according to (1.2).

$$Li^6 + n \rightarrow T + He^4 + 4.8\ MeV \tag{1.2a}$$
$$Li^7 + n \rightarrow T + He^4 + n - 2.5\ MeV \tag{1.2b}$$

This is the reason that future fusion power plants will have Lithium blanket which will breed Tritium. There is estimated 80 million tons of Lithium in the world and with a conversion rate of 0.86 GWy/ton in a fusion power plant there is enough Lithium to fuel the world's current energy demand for 4000 years. This time can be considerably shorter if Lithium is being used in other applications (Lithium is a key component in today's batteries). However, there is a large amount of Lithium in the world's oceans, billions of tons. The other fuel source for the fusion process, Deuterium is luckily much more accessible as it can be procured by extracting it from heavy water through electrolysis. Heavy water can be extracted from fresh water. Since it is extracted from water the deuterium reserves are vast, 1 part in 6400 in water. As the fuel for a pure Deuterium-fueled power plant is much more accessible the hope is that a Deuterium power plant might be feasible some day. Because D-T is the fuel for a future power plant it would at first sight reasonable experiment with it on a regular basis. However, the experiments with D-T are few and far between because of the high number of energetic neutrons these experiments create. These neutrons activate the tokamak walls and they become radioactive. Therefore, most experiments today are run with hydrogen, deuterium and more rarely with Helium. Even though this is a different fuel composition that will be used for a future power plant, nevertheless these plasmas display similar behavior as to D-T plasma.

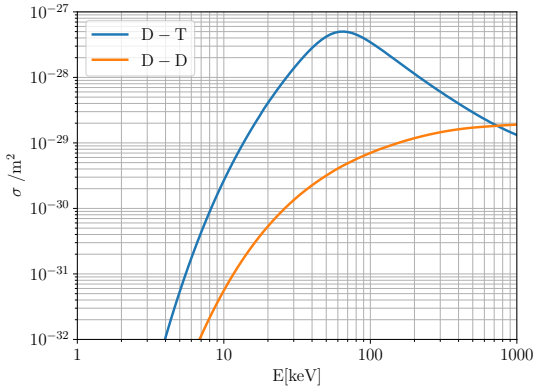

Figure 1.2: *Cross section for D-D and D-T reactions as a function of the nuclei energy*

.

Another major advantage of fusion reactors are that they are intrinsically safe. The maximum energy that can be released in an accident is the total energy stored in the reactor at any time. An accidental loss of the confinement leads to the plasma rapidly distinguish. Moreover the amount of tritium, a radioactive element, is very small, roughly the weight of a stamp.

1.2 Different approaches to fusion

There are several fields of research trying to obtain fusion power production for instance inertial confinement fusion and magnetic confined fusion. In inertial confinement fusion the material is heated and compressed extremely quickly so that it reaches conditions for fusion. The material is held together by the inertia of the fuel itself, hence the name. The fuel is prepared in a small pellet with a radius of a few millimeters and put in a so called hohlraum. There it is bombarded by high energetic laser beams that compress the pellet. As the pellet is compressed instabilities can occur and the fusion criteria might not be achieved. This is an ongoing field of research and relies heavy on the development of more powerful laser beams.

The other approach is to use strong magnetic fields to confine the fuel, the most researched device is the tokamak, which is also the focus for this thesis. The tokamak is a doughnut shaped chamber where the nuclei are contained with a strong magnetic field. This concept has shown its potential in several experiments and much research is put into optimizing it. The nuclei are in a state called plasma in the tokamak. Plasma is a hot ionized gas containing charged and neutral particles that is quasi-neutral and shows collective behavior. Figure (1.2) shows that the particles need to have a high temperature, in the order of 10-25 keV (100-300 million degrees), to achieve fusion. In a future fusion power plant the majority of the heating will come from the 3,5 MeV He^4-particles released in the fusion process which will be confined by the magnetic field and slowed down by collisions on the bulk plasma and thereby heat it. However, the particles need to be initially heated for the fusion process to start. There are a number of methods available for heating the plasma in

a future power plant and these have been successfully tested in current experiments. The plasma in a tokamak is heated ohmically by the current, at higher temperature the efficiency of the ohmic heating is lowered as the resistivity gets small. Other heating schemes are needed such as the Neutral Beam Injection (NBI) where highly energetic beams of neutrals are injected into the plasma. NBI functions both as an energy and particle source. Radio frequency waves heat the plasma by interactions through resonances with the particles.

In this thesis, we will focus on magnetic confined plasma in a toroidal geometry, specifically in a tokamak. The outline of this kappa is as follows. In chapter (2) we will describe the plasma in four different ways. First we will discuss the single particle motion in a plasma, secondly the kinetic description of the plasma, thirdly the two-fluid approach and finally one-fluid approach or magneto-hydrodynamics (MHD) as it is called. We will also discuss the method of taking the gyroaverage for particles in a magnetically confined plasma and two models which take advantage of this, gyrokinetics and gyrofluids. In chapter (3) we will discuss turbulent transport in more detail and its implication for the efficiency for a fusion power plant. Finally in chapter (4) we will give a brief summary of the appended papers.

CHAPTER 2

THEORETICAL DESCRIPTIONS OF PLASMAS

In this section we will describe the plasma in four different ways, representing four different levels of approximation. The simplest is the single particle description in which all particles are treated separately and this will give an intuitive feeling for some of the phenomena in the plasma. In this approximation the electromagnetic fields are prescribed and does not change depending on the movements of the particles. In principle the evolution of a closed system of charged particles can be determined by calculating the electromagnetic forces acting upon them from each other and external forces (from a magnetic field). However, even though a fusion plasma is about 10^5 times less dense than air, the number of particles per cubic meter is about 10^{19}. The interactions between all of these particles present an unfeasible computational problem. Hence, the need for models that treat the particles in a more course grain terms, which is why we introduce the three main models of plasma dynamics, the Vlasov theory (or kinetic theory), two-fluid theory and magnetohydrodynamics (MHD). In all of these models the electromagnetic fields are calculated self-consistently with Maxwell's equations. The Vlasov model is the most detailed of the models and follows the evolution of the electron and ion velocity distribution functions. The two fluid model (or multifluid) is the intermediate of the three and describe the plasma as two or more interacting fluids. The MHD model is the least detailed which approximates the plasma as a single fluid. All of these models have different benefits and drawbacks which we will discuss.

2.1 Single particle movement

It is advantageous to discuss the motion of a single particle in the plasma to get an understanding of some of the phenomena that occurs there. Magnetic confinement relies on a strong magnetic field which creates a Lorentz force.

$$\boldsymbol{F}_L = Ze(\boldsymbol{E} + \boldsymbol{v} \times \boldsymbol{B}) \tag{2.1}$$

Here $\boldsymbol{F}_L$ is the Lorentz force acting upon a particle, Ze is the charge of the particle, $\boldsymbol{E}$ is the electric field, $\boldsymbol{v}$ is the particles velocity and $\boldsymbol{B}$ is the magnetic field.

As a first step we study the case with a stationary, homogeneous magnetic field and the absence of an electric field. In this case the velocity parallel with the magnetic field is constant as the force only act perpendicular to the field. Therefore, the particle will not gain any energy. The equation of motion for the two directions perpendicular to the magnetic field becomes:

$$\ddot{v}_{\perp_1} + \left(\frac{qB}{m}\right)^2 v_{\perp_1} = 0 \tag{2.2}$$

$$\ddot{v}_{\perp_2} + \left(\frac{qB}{m}\right)^2 v_{\perp_2} = 0 \tag{2.3}$$

here the dots denote derivatives with respect of time and $\perp_1$, $\perp_2$ denotes the two orthogonal axis perpendicular to the magnetic field. Eq. (2.2) and Eq. (2.3) describes a harmonic oscillator with the oscillation frequency.

$$\omega_c = \frac{|Ze|B}{m} \tag{2.4}$$

The cyclotron frequency describe one of the fastest phenomena in the plasma. Because we generally are interested in processes that take place on longer time scales, it is common to adopt a multi timescale expansion thereby the gyromotion is averaged over. This simplifies the equations which we will describe in more detail later. The particles motion becomes a helix around the magnetic field. The radius of this motion is called the Larmor radius:

$$r_L = \frac{v_\perp}{\omega_c} \tag{2.5}$$

The Larmor radius is small compared to the size a modern tokamak experiment. This means that the particles are ”bound” to the magnetic field lines, greatly limiting the transport perpendicular to the magnetic field lines. However, while the gyromotion limits the motion of charged particles in the direction perpendicular to the magnetic field, they can freely stream along the magnetic field, i.e. they are confined. The perhaps at first sight simplest solution would be to bend the magnetic field lines into a torus, such that the particles would travel in circles in the toroidal direction, i.e. along the field lines. Unfortunately, this will not work as it exist "drifts" from the magnetic field lines. We will first introduce these drifts and later describe a concept to handle them.

As a second step we introduce a general constant force; $\boldsymbol{F}$. If a part of the force is parallel to the magnetic field the particle will accelerate forever, this will of course not happen in a real plasma as there are other mechanisms to stop that. If the force has a component perpendicular to the magnetic field this will give rise to a drift velocity. This velocity will drift the particle from a given magnetic field line.

$$\boldsymbol{v}_d = \frac{\boldsymbol{F}_\perp \times \boldsymbol{B}}{ZeB^2} \tag{2.6}$$

The discussion above has been done with a straight magnetic field. Before introducing more realistic magnetic fields we first need to introduce the concepts of guiding center and gyro-averaging. As we have seen, a charged particle gyrates around a magnetic field line, the center of this motion is called the guidingcenter. The position of the particle can be split up to a gyrocenter part and a fast moving gyration part.

$$\boldsymbol{x} = \boldsymbol{x}_{gc} + \boldsymbol{x}_L, \boldsymbol{v} = \boldsymbol{v}_{gc} + \boldsymbol{v}_L \tag{2.7}$$

here we have $\boldsymbol{v}_{gc}$ as the velocity of the guiding-center which the particle gyrates around. $\boldsymbol{v}_L$ is the velocity of the gyration. The gyroaverage is defined as

$$\langle f \rangle_{\boldsymbol{x}_{gc}} = \frac{1}{2\pi} \oint f(\boldsymbol{x}_{gc}, v_\parallel, v_\perp, \gamma) d\gamma \tag{2.8}$$

here γ is the gyroangle. $\boldsymbol{x}_{gc}, v_\parallel$ and $v_\perp$ are kept constant during the averaging. When we have a constant magnetic field and no external forces, Eq. (2.8) becomes an average over the perpendicular motion. Therefore, $\langle \boldsymbol{x}_L \rangle_{\boldsymbol{x}_{gc}} = 0$, $\langle \boldsymbol{v}_\perp \rangle_{\boldsymbol{x}_{gc}} = 0$ and $\langle \boldsymbol{x} \rangle_{\boldsymbol{x}_{gc}} = \boldsymbol{x}_{gc}$. However, with an external force we get a drift. The velocity of the guiding-center as $\boldsymbol{v}_{gc} = v_\parallel \hat{\boldsymbol{b}} + \boldsymbol{v}_d$ with the drift velocity from (2.6). Here we can notice that a straight magnetic field line will not confine the particle if an external force exist.

2.2 Slowly varying magnetic field

Up to this point, we have assumed a homogeneous, static magnetic field but we shall now consider a spatial dependence in the magnetic field. This is important for the tokamak as its topology makes it impossible to achieve a homogeneous magnetic field. This is due to the fact that the coils that create the toroidal magnetic field are much closer together on the inside than on the outside of the tokamak. We are only going to look at the case when the magnetic field changes weakly, i.e. the characteristic length of the change in the magnetic field must be much larger than the Larmor radius, which is an necessity for a magnetic confined plasma. We expand the magnetic field around the guiding center:

$$\boldsymbol{B}(\boldsymbol{x}) = \boldsymbol{B}(\boldsymbol{x}_{gc}) + \boldsymbol{x}_L \cdot \nabla \boldsymbol{B}(\boldsymbol{x}_{gc}) + \mathcal{O}(r_L^2) \tag{2.9}$$

here again we have $\boldsymbol{x} = \boldsymbol{x}_{gc} + \boldsymbol{x}_L$. The second term in the equation is much smaller if the magnetic field changes slowly compared to the Larmor radius. This can be seen by taking the ratio of the two terms and denote the characteristic change of the magnetic field as L, then $\nabla \sim 1/L$, hence

$$\frac{|\boldsymbol{x}_L \cdot \nabla \boldsymbol{B}(\boldsymbol{x}_{gc})|}{|\boldsymbol{B}(\boldsymbol{x}_{gc})|} \sim \frac{r_L}{L} \ll 1 \tag{2.10}$$

This holds in a representative fusion reactor. The effective force from the first order change in the magnetic field can be written as:

$$\boldsymbol{F}_{eff} = \langle Ze\boldsymbol{v} \times (\boldsymbol{x}_L \cdot \nabla \boldsymbol{B}(\boldsymbol{x}_{gc})) \rangle_{\boldsymbol{x}_{gc}} \tag{2.11}$$

if we calculate the integral in Eq. (2.8) we end up with:

$$\boldsymbol{F}_{eff} = -mv_{\parallel}^2\boldsymbol{\kappa} - \mu\nabla B \tag{2.12}$$

here $\boldsymbol{\kappa} = \hat{\boldsymbol{b}} \cdot \nabla\hat{\boldsymbol{b}}$ is the magnetic curvature and $\mu = mv_{\perp}^2/(2B)$ is the magnetic moment. These two effective forces have both physical representation. The first term, is a centrifugal force caused by the curvature in the magnetic field. The magnetic moment is an adiabatic invariant and as such it can be interpreted as a property of the guiding center. The kinetic energy of a particle can be written as $mv_{\parallel}^2/2 + \mu B$, thus we can look at the last term as an effective potential, U. This potential will give rise to a force when the particle crosses from higher or lower magnetic field, $\boldsymbol{F} = -\nabla U$, which represent the second term in Eq. (2.12). This term is called the mirror force as it reflects particles with insufficient kinetic energy to overcome the potential of a stronger magnetic field.

From Eq. (2.6) we can calculate an associated drift velocity from the effective force. If we also let the electric field to be non-zero, $\boldsymbol{E} \neq 0$, with the assumption that the electric field is close to constant over one particle gyration. The velocity for the guiding center becomes

$$\boldsymbol{v}_{gc} = v_{\parallel}\hat{\boldsymbol{b}} + \boldsymbol{v}_d \tag{2.13}$$

where the parallel velocity $v_{\parallel}$ is computed from the parallel component of the force $\boldsymbol{F} = Ze\boldsymbol{E} + \boldsymbol{F}_{eff}$. We get the drift velocity from (2.6)

$$\boldsymbol{v}_d = \frac{\boldsymbol{E}\times\boldsymbol{B}}{B^2} + \frac{v_{\perp}^2}{2\omega_c}\hat{\boldsymbol{b}}\times\nabla logB + \frac{v_{\parallel}^2}{\omega_c}\hat{\boldsymbol{b}}\times\boldsymbol{\kappa} \tag{2.14}$$

where the first term is the so called ExB-drift, the second term is associated with the change in the magnetic field and the third is the curvature-drift. The second term is small due to the ratio r_L/L, here L is the characteristic length of the change in the magnetic field. An interesting thing to notice for the two magnetic drifts, there is a charge dependence, hence the ions and electrons will drift in opposite directions. For the ExB-drift however we have no dependence of the charge, thus ions and electrons will drift in the same direction and at the same speed as it is independent of mass.

The drift is small compared to the parallel motion of the particles along the magnetic field, however for the confinement these drifts are important.

2.2.1 Toroidal geometry

To discuss a toroidal geometry, as present in a tokamak, we first need to present a toroidal coordinate system, as shown in Figure (2.1). The coordinate system (Z,R,ϕ), where R is the distance from the symmetric center, Z the height from symmetric plane and ϕ the azimuthal angle. First we will discuss a magnetic field with only a toroidal component, $\boldsymbol{B} = B\hat{\phi}$. This can be created by a current in a long wire passing through origo in the $\hat{Z}$-direction. Amperes law gives the strength of the magnetic field

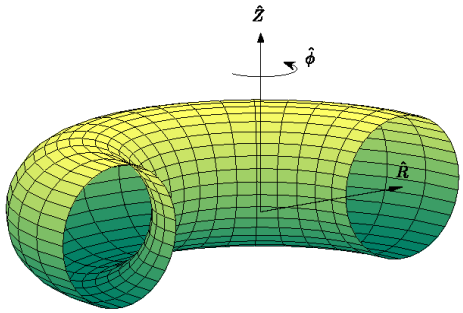

Figure 2.1: *Toroidal geometry and coordinates*

$$B = \frac{\mu_0 I}{2\pi R}\hat{\phi} \tag{2.15}$$

where I is the total current in the wire and R is the length to the $\hat{z}$-axis. It is clear that the magnetic field decays with R, $B \sim R^{-1}$. This is the same dependency as a realistic toroidal magnetic field in a tokamak which has its toroidal magnetic field created by external currents in coils wound around the minor radia. We can use the discussion in the previous section to state the effective force on the particles in this magnetic field. The effective force on the guiding center, in this toroidal coordinate system, becomes.

$$\boldsymbol{F}_{eff} = \left(\frac{mv_\parallel^2}{R} + \frac{\mu B}{R}\right)\hat{R} \tag{2.16}$$

with this effective force we get the drift as:

$$\boldsymbol{v}_d = \left(v_\parallel^2 + \frac{v_\perp^2}{2}\right)\frac{m}{ZeBR}\hat{Z} \tag{2.17}$$

If we assume that $v_\parallel \sim v_\perp$, we get

$$\boldsymbol{v}_d \sim \frac{r_L}{R}\left(v_\parallel + \frac{v_\perp}{2}\right)\hat{Z} \tag{2.18}$$

Here we see that the drift will be just a fraction of the velocities as r_L/R is small. To get the drift we need to get an average over the whole toroidal motion. As the particles are locked to the magnetic field lines, this is trivial in the case with a magnetic field with only a toroidal component. In the zeroth order in r_L/R we do not get a drift and the particles are confined by a purely toroidal magnetic field. However, as in a real tokamak the ratio r_L/R is non zero it is clear that the particles will drift from their magnetic field in the $\hat{Z}$-direction.

In order to solve this problem a poloidal magnetic field needs to be added and the tokamaks solution to this is to create a current in the plasma that adds the poloidal magnetic field. The current in the tokamak is created by a large transformer at the center of the machine. The transformer creates one of the limitations on how long an experiment in a tokamak can run as its core gets saturated. This solution creates a helical magnetic field around the toroidal surfaces. These surfaces are known as flux-surfaces. As these flux-surfaces by no means need to be (or are)

circular we need to define a new type of coordinate system. A new radial coordinate, the flux surface label ρ_t which defines a flux-surface, i.e. is constant on them and varies between different flux-surfaces. The flux-label can be defined by the poloidal or the toroidal magnetic flux, in this thesis we will define it as dependent on the toroidal magnetic flux, as denoted by the "t" in ρ_t. The normalized ρ_t is defined as:

$$\rho_t = \sqrt{\frac{\Phi - \Phi_{ax}}{\Phi_{sep} - \Phi_{ax}}} \tag{2.19}$$

Here Φ, Φ_{ax}, Φ_{sep} is the toroidal magnetic flux, the toroidal magnetic flux at the magnetic axis and at the separatrix, respectively. They are defined by:

$$\Phi = \int_{S_t} \boldsymbol{B} \cdot d\boldsymbol{S}_t \tag{2.20}$$

To determine the cumulative results of the drift for these helical magnetic fields is more difficult compared to the purely toroidal fields. We have to study the drift over several laps around the toroidal orbits. For these drifts to cancel each other out we need to look at the average drift over the particle path as it move on the helical flux-surface until it ends up at its initial poloidal position. We describe this path as the length l. If the particle is going to be confined we need to have no net drift in the radial direction, i.e. ρ_t. This can be expressed with the integral.

$$\oint \boldsymbol{v}_d \cdot \boldsymbol{\nabla} \rho_t dl = 0 \tag{2.21}$$

The easiest way to explain how this equation holds true for particles in a tokamak with helical magnetic field is to draw how a particle moves around. In Figure (2.2) a) we plot the cross-section of a particles' movement. The helical magnetic field make the particle move from the outer part of the tokamak (right part of the figure) to the inner (left part of the figure). As the drift is in the $\hat{Z}$ according to Eq. (2.18) at the upper part of the figure the particle is drifting to an inner fluxsurface. At the bottom it drifts outwards again. Hence, the average means that the particle end up at the same fluxsurface.

As the magnetic field strength varies across the major radius the particles will feel a stronger magnetic force as they move closer to the center of the torus. As previously discussed this means that some particles with insufficient parallel velocity will turn back. This can be described as $mv_{\|}^2 < \mu B_{max}$, there B_{max} is the maximum field strength along the magnetic field line. This magnetic mirror force creates two distinct types of particles, the ones with sufficient parallel velocity, $mv_{\|}^2 > \mu B_{max}$ which will make the full orbit along the field line, passing particles. The other type of particles are the ones with too low parallel velocity, these will not make a full orbit and will bounce back and forth, therefore they are called trapped particles. Their orbits are displayed in Figure (2.2) b) and they are located on the low field side of the tokamak. These particles give rise to an instability called the Trapped Electron Mode (TEM).

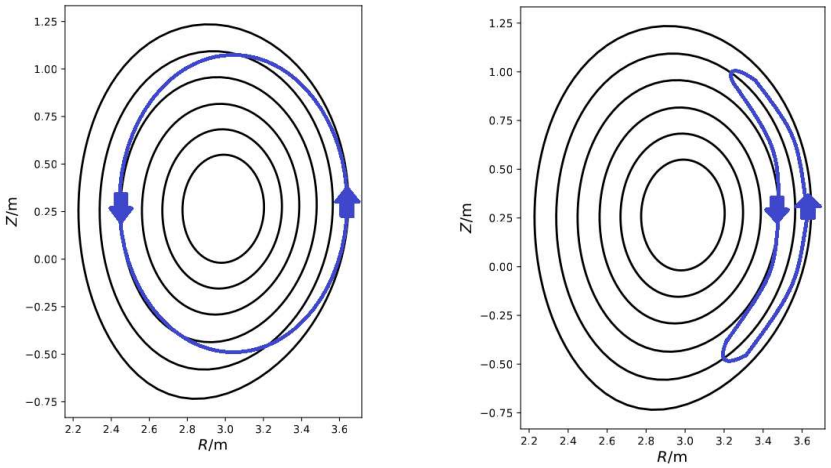

(a) Passing particles **(b)** Trapped particles

Figure 2.2: a) The drift of passing particles. At the top part of the tokamak the particle is drifting towards the centre, at the bottom part it is drifting outwards. b) The blue line depicts trapped electrons in a ”banana”-orbit

2.3 Kinetic description

The kinetic description of plasmas is a statistical description of a system of identical particles. We introduce the distribution function, $f(\boldsymbol{x}, \boldsymbol{v}, t)$ which describes the probability to find a particle with velocity $\boldsymbol{v}$ and position $\boldsymbol{x}$ at time t in phase space. The distribution function is closely linked to thermodynamic quantities of the plasma, by integrating the distribution function over the velocity we get the particle density,

$$n(\boldsymbol{x}, t) = \int f(\boldsymbol{x}, \boldsymbol{v}, t) d^3v \tag{2.22}$$

This procedure is called taking velocity moments (or only moments) of the distribution function. Eq. (2.22) is the zeroth moment, we multiply the distribution function with $\boldsymbol{v}^0$ and perform the integrating. Other thermodynamic quantities can be calculated by taking higher order moments:

$$\textit{Mean velocity} = \boldsymbol{u}(\boldsymbol{x}, t) = \frac{1}{n} \int \boldsymbol{v} f(\boldsymbol{x}, \boldsymbol{v}, t) d^3v \tag{2.23a}$$

$$\textit{Pressure tensor} = \overleftrightarrow{\boldsymbol{P}}(\boldsymbol{x}, t) = m \int \boldsymbol{v}'\boldsymbol{v}' f(\boldsymbol{x}, \boldsymbol{v}, t) d^3v \tag{2.23b}$$

$$\textit{Heat flux vector} = \boldsymbol{Q}(\boldsymbol{x}, t) = \int \frac{m v'^2}{2} \boldsymbol{v}' f(\boldsymbol{x}, \boldsymbol{v}, t) d^3v \tag{2.23c}$$

We have decomposed the velocity: $\boldsymbol{v} = \boldsymbol{u}(\boldsymbol{x}, t) + \boldsymbol{v}'(\boldsymbol{x}, t)$, here $\boldsymbol{v}'(\boldsymbol{x}, t)$ is the random part of a given velocity, hence $\int \boldsymbol{v}' f d^3v = 0$. We now have the

connection between the distribution function and thermodynamic quantities, we will now proceed to create a framework to determine the distribution function. To do this we will treat the macroscopic forces (such as the Lorentz force from the electromagnetic fields) and microscopic forces such as from collisions. The change of particles in a volume in phase-space is equal to the flux in (or out), which means we do not have any sources or sinks in the box (ignoring fusion processes for now). This can described as

$$\frac{df(\boldsymbol{x},\boldsymbol{v})}{dt} = \frac{\partial f}{\partial t} + \boldsymbol{v}\cdot\frac{\partial f}{\partial \boldsymbol{x}} + \boldsymbol{a}\cdot\frac{\partial f}{\partial \boldsymbol{v}} = 0 \tag{2.24}$$

which is the Vlasov or the collisionless Boltzmann equation and is the basis for many of the models in plasma physics. The acceleration comes from the force $\boldsymbol{a} = \frac{Ze}{m}(\boldsymbol{E} + \boldsymbol{v}\times\boldsymbol{B})$. This force is determined by the Maxwell's equations:

$$\nabla\cdot\boldsymbol{E} = \sum_\sigma Z_\sigma e\int f_\sigma d^3v \tag{2.25a}$$

$$\nabla\cdot\boldsymbol{B} = 0 \tag{2.25b}$$

$$\nabla\times\boldsymbol{E} = -\frac{\partial \boldsymbol{B}}{\partial t} \tag{2.25c}$$

$$\nabla\times\boldsymbol{B} = \sum_\sigma Z_\sigma e\int \boldsymbol{v} f_\sigma d^3v + \frac{\partial \boldsymbol{E}}{\partial t} \tag{2.25d}$$

Here we added σ to identify each particle species. For certain processes the Vlasov equation need to be augmented by adding a collision operator on the right hand side.

$$\frac{\partial f_\sigma}{\partial t} + \boldsymbol{v}\cdot\frac{\partial f_\sigma}{\partial \boldsymbol{x}} + \boldsymbol{a}\cdot\frac{\partial f_\sigma}{\partial \boldsymbol{v}} = \sum_\alpha C_{\sigma\alpha}(f_\sigma) \tag{2.26}$$

This is the collisional kinetic equation, called the Boltzmann equation. Here $C_{\sigma\alpha}$ is the rate of change for f_σ due to collisions between species σ and α.

2.4 Two fluid-models

The kinetic description of the plasma can be computationally heavy. A different approach to study the plasma is to look at it as a composite of fluids (instead of a group of discrete particles). This can be done by taking moments of the Boltzmann equation, Eq. (2.26) which will create a set of partial differential equations which will couple the mean quantities, presented in Eq. (2.22) and (2.23), such as $n(\boldsymbol{x},t), \boldsymbol{u}(\boldsymbol{x},t)$ etc. If we take the first moment of the Boltzmann equation by multiplying by unity and integrating over velocity space.

$$\int\left(\frac{\partial f_\sigma}{\partial t} + \boldsymbol{v}\cdot\frac{\partial f_\sigma}{\partial \boldsymbol{x}} + \boldsymbol{a}\cdot\frac{\partial f_\sigma}{\partial \boldsymbol{v}}\right)d^3v = \sum_\alpha\int C_{\sigma\alpha}(f_\sigma)d^3v \tag{2.27}$$

For the two terms on the left hand side the integral commutes with the time and space derivatives as $\boldsymbol{x},\boldsymbol{v}$ and t is independent variables. We can rewrite

the third term so we get $\int \frac{\partial f_\sigma}{\partial \boldsymbol{v}} \cdot (\boldsymbol{a} f_\sigma) d^3v$. This is the volume integral of a divergence in velocity space, hence we can use Gauss theorem to rewrite it: $\oint \boldsymbol{a} f_\sigma \cdot d\boldsymbol{S}$. It is easy to understand that his term will vanish, $f_\sigma \to 0$ as $|v| \to \infty$. This is stating the fact that the probability to find a particle with infinite velocity is zero. The right hand side is equal to zero as collisions can not change the number of particles. Using this we get:

$$\frac{\partial n_\sigma}{\partial t} + \nabla \cdot (n_\sigma \boldsymbol{u}_\sigma) = 0 \tag{2.28}$$

This is the continuity equation, which is the first equation that constitutes the basis for the two fluid-model. Let us take the first moment of the Boltzmann equation by multiplying it with $\boldsymbol{v}$ and integrating over the velocity:

$$\int \boldsymbol{v} \left(\frac{\partial f_\sigma}{\partial t} + \boldsymbol{v} \cdot \frac{\partial f_\sigma}{\partial \boldsymbol{x}} + \boldsymbol{a} \cdot \frac{\partial f_\sigma}{\partial \boldsymbol{v}} \right) d^3v = \sum_\alpha \int \boldsymbol{v} C_{\sigma\alpha}(f_\sigma) d^3v \tag{2.29}$$

We may rewrite this by using the following

1. Again use the fact the integral commutes with both the time a space derivative for the two first terms on the left hand side
2. Write the velocity as $\boldsymbol{v} = \boldsymbol{u}(\boldsymbol{x}, t) + \boldsymbol{v}'(\boldsymbol{x}, t)$, here $\boldsymbol{v}'(\boldsymbol{x}, t)$ is the random part of a given velocity, hence $\int \boldsymbol{v}' f_\sigma d^3v = 0$.
3. When integrating the third term on the left hand side use the fact that

$$\left(\frac{\partial v_i}{\partial v_j} \right) = \delta_{ij} \tag{2.30}$$

Here δ_{ij} is the kronecker-delta. By using this we can rewrite (2.29).

$$\frac{\partial (n_\sigma \boldsymbol{u}_\sigma)}{\partial t} + \frac{\partial}{\partial \boldsymbol{x}} \cdot \int (\boldsymbol{v}'\boldsymbol{v}' + \boldsymbol{v}'\boldsymbol{u}_\sigma + \boldsymbol{u}_\sigma \boldsymbol{v}' + \boldsymbol{u}_\sigma \boldsymbol{u}_\sigma) f_\sigma d^3v - \int \boldsymbol{a} f_\sigma d^3v = \sum_\alpha \boldsymbol{R}_{\sigma\alpha} \tag{2.31}$$

The two terms with a single mean velocity $\boldsymbol{u}_\sigma$ in the first integral disappears as $\int \boldsymbol{v}' f_\sigma d^3v = 0$ and $\boldsymbol{u}_\sigma$ is independent of v. We can also see that the first term in the first integral is the pressure tensor, defined in Eq. (2.23b).

It is a common assumption to take f_σ to be an isotropic function in v as this simplifies the pressure tensor greatly. However this is done purely for convenience and for real distribution functions isotropy is far from guaranteed. Collisions in the system drives the distribution function towards isotropy but a sparse hot plasma usually does not have enough collisions. We are going to leave the pressure tensor by its definition from Eq. (2.23b). The right hand side of Eq. (2.31), $\boldsymbol{R}_{\sigma\alpha}$ is the net frictional drag force of species σ due to collision with species α. As a species can not exert a net force upon itself, $\boldsymbol{R}_{\sigma\sigma} = 0$. Due to the conservation of momentum it follows that $\boldsymbol{R}_{\alpha\sigma} + \boldsymbol{R}_{\sigma\alpha} = 0$.

If we put this all together and assume the only acceleration is created by the Lorentz Force we get the so called momentum equation:

$$n_\sigma m_\sigma \frac{d\boldsymbol{u}_\sigma}{dt} = n_\sigma Z_\sigma e(\boldsymbol{E} + \boldsymbol{u}_\sigma \times \boldsymbol{B}) - \nabla \cdot \overleftrightarrow{\boldsymbol{P}}_\sigma + \sum_\alpha \boldsymbol{R}_{\sigma\alpha} \tag{2.32}$$

Here we used the operator d/dt which is defined as the convective derivative

$$\frac{d}{dt} = \frac{\partial}{\partial t} + \boldsymbol{u}_\sigma \cdot \nabla \tag{2.33}$$

which describes the rate of change seen by an observer moving with the mean fluid velocity $\boldsymbol{u}_\sigma$.

We will now briefly look at the second moment of the Boltzmann equation. This is done by multiplying the Boltzmann equation, Eq. (2.26), with $m_\sigma v^2/2$

$$\int \frac{m_\sigma v^2}{2} \left(\frac{\partial f_\sigma}{\partial t} + \boldsymbol{v} \cdot \frac{\partial f_\sigma}{\partial \boldsymbol{x}} + \boldsymbol{a} \cdot \frac{\partial f_\sigma}{\partial \boldsymbol{v}} \right) d^3v = \sum_\alpha \int \frac{m_\sigma v^2}{2} C_{\sigma\alpha}(f_\sigma) d^3v \tag{2.34}$$

This is the starting point for the derivation of the energy conservation equation, (a derivation can be found in [1] among others)

$$\frac{3}{2}\frac{dP_\sigma}{dt} + \frac{5}{2} P_\sigma \nabla \cdot \boldsymbol{u}_\sigma = -\nabla \cdot \boldsymbol{Q}_\sigma + \sum_\alpha \left[\boldsymbol{R}_{\sigma\alpha} \cdot \boldsymbol{u}_\sigma - \left(\frac{\partial W}{\partial t} \right)_{E\sigma\alpha} \right] \tag{2.35}$$

The last term on the right hand side is the rate which the species α collisionialy transfers to species σ and is defined as:

$$\left(\frac{\partial W}{\partial t} \right)_{E\sigma\alpha} = -\sum_\alpha \int \frac{m_\sigma v^2}{2} C_{\sigma\alpha}(f_\sigma) d^3v \tag{2.36}$$

We also have the heat flux defined in Eq. (2.23a).

The equations (2.28), (2.32), and (2.35) are a set of coupled differential equations. These are called the Braginskii equations [2]. One very important thing to notice about these equations is that a pattern appears. When we took the zeroth moment to derive an equation for the density we got a term with the mean velocity. In the same way when we took the first moment to derive an equation for velocity we got a term with pressure. And finally for the second moment, in the equation for the energy we got a higher order term as well. This is an open system. To create a system of equation which can be solved some closure is needed. This can be done in several ways, some of them are assuming adiabatic or isothermal processes. More advanced closures have been developed which are valid also in the weak collisionality limit relevant to the core region of fusion plasmas. An example is the fluid model developed at Chalmers [48] which has been successfully used to analyze and predict tokamak experiments at JET. The equations (2.28), (2.32), and (2.35) are the fundamental equations for two-fluid models. The aforementioned equations can be easily generalized for more ion species, for example to take into account a second main ion species, as in a Deuterium-Tritium plasma, or impurities.

2.5 Magnetohydrodynamics

As the plasma is composed of ions an electrons it is natural to describe the plasma as two fluids. We can however go one step further and describe all particles in the plasma as one fluid. This model is the simplest we are going to look at and it is called Magnetohydrodynamics (MHD). For this model to be valid the plasma needs to be collision dominated and it include low-frequency, long-wavelength, magnetic behavior of the plasma. MHD has a macroscopic point of view compared to the kinetic theory and the two-fluid model. In the following section we will derive the so called Grad-Shafranov equation which defines the static magnetic geometry with nested flux surfaces. We use flux coordinate system in our transport simulations.

The characteristic properties for the MHD model are, the total mass density ρ, the total charge density ρ_c, the center of mass velocity $\boldsymbol{U}$ and the current density $\boldsymbol{I}_p$:

$$\rho \equiv m_i n_i + m_e n_e \tag{2.37a}$$
$$\rho_c \equiv e(Z_i n_i - n_e) \tag{2.37b}$$
$$\boldsymbol{U} \equiv \frac{m_i n_i \boldsymbol{u}_i + m_e n_e \boldsymbol{u}_e}{m_i n_i + m_e n_e} \tag{2.37c}$$
$$\boldsymbol{I_p} \equiv e(Z_i n_i \boldsymbol{u}_i - n_e \boldsymbol{u}_e) \tag{2.37d}$$

Here $m_i, m_e, n_i, n_e, \boldsymbol{u}_i$ and $\boldsymbol{u}_e$ are the masses, densities and fluid velocities for the ions and electrons. If we use the assumption of quasi neutrality, i.e $Z_i n_i \approx n_e$, we notice that the charge density vanishes.

The derivation of the equations that governs MHD are similar to the one done for the two fluid model in the previous section. This is done by again taking moments of the Boltzmann equation, Eq. (2.26), but now multiplying it with m_σ and take the sum over all particle species. The MHD continuity equation is trivially derived.

$$\frac{\partial \rho}{\partial t} + \nabla \cdot (\rho \boldsymbol{U}) = 0 \tag{2.38}$$

This equations states mass conservation. The momentum equation is derived by taking the first moment and take the sum over all species:

$$\frac{\partial}{\partial t} \sum_\sigma m_\sigma \int \boldsymbol{v} f_\sigma d^3v + \frac{\partial}{\partial \boldsymbol{x}} \cdot \Sigma_\sigma \int m_\sigma \boldsymbol{v}\boldsymbol{v} f_\sigma d^3v + \sum_\sigma q_\sigma \int \boldsymbol{v} \frac{\partial}{\partial \boldsymbol{v}} \cdot [(\boldsymbol{E} + \boldsymbol{v} \times \boldsymbol{B}) f_\sigma] = 0 \tag{2.39}$$

Here we have zero on the right hand side as $\boldsymbol{R}_{\sigma\alpha} + \boldsymbol{R}_{\alpha\sigma} = 0$, the plasma can not add to its own momentum. In MHD we will define the relative velocities compared to the center of mass velocity, $\boldsymbol{v}_\sigma = \boldsymbol{U} + \boldsymbol{v}^*_\sigma$. The integral in the second term can then be written as,

$$\sum_\sigma \int m_\sigma \boldsymbol{v}_\sigma \boldsymbol{v}_\sigma f_\sigma d^3v = \sum_\sigma \int m_\sigma (\boldsymbol{U} + \boldsymbol{v}^*_\sigma)(\boldsymbol{U} + \boldsymbol{v}^*_\sigma) f_\sigma d^3v = \sum_\sigma \int m_\sigma \boldsymbol{v}^*_\sigma \boldsymbol{v}^*_\sigma f_\sigma d^3v + \rho \boldsymbol{U}\boldsymbol{U} \tag{2.40}$$

where the parts with a single $\boldsymbol{v}_\sigma^*$ are discarded as $\sum_\sigma \int m_\sigma \boldsymbol{v}_\sigma^* f_\sigma d^3v = 0$. We define the MHD pressure tensor which is given by the random velocities relative to $\boldsymbol{U}$.

$$\overleftrightarrow{\boldsymbol{P}}^{MHD} = \sum_\sigma \int m_\sigma \boldsymbol{v}_\sigma^* \boldsymbol{v}_\sigma^* f_\sigma d^3v \tag{2.41}$$

The third term in Eq. (2.39) can be integrated by parts, which we can use to get the following expression:

$$\frac{\rho \boldsymbol{U}}{\partial t} + \nabla \cdot (\rho \boldsymbol{U}\boldsymbol{U}) = \left(\sum_\sigma n_\sigma q_\sigma \right) \boldsymbol{E} + \boldsymbol{I_p} \times \boldsymbol{B} - \nabla \overleftrightarrow{\boldsymbol{P}}^{MHD} \tag{2.42}$$

Here we can use the quasi neutrality criteria and see that the term with the electric field vanishes. The two first terms can be expanded:

$$\begin{aligned} \frac{\rho \boldsymbol{U}}{\partial t} + \nabla \cdot (\rho \boldsymbol{U}\boldsymbol{U}) &= \underbrace{\left(\frac{\partial \rho}{\partial t} + \nabla \cdot (\rho \boldsymbol{U}) \right)}_{\text{continuity equation}} \boldsymbol{U} + \rho \frac{\partial \boldsymbol{U}}{\partial t} + \rho \boldsymbol{U} \cdot \nabla \boldsymbol{U} \\ &= \rho \left(\frac{\partial \boldsymbol{U}}{\partial t} + \boldsymbol{U} \cdot \nabla \boldsymbol{U} \right) \end{aligned} \tag{2.43}$$

Now we are ready to write the momentum equation for MHD in its standard from

$$\rho \frac{D\boldsymbol{U}}{Dt} = \boldsymbol{I}_p \times \boldsymbol{B} - \nabla \cdot \overleftrightarrow{\boldsymbol{P}}^{MHD} \tag{2.44}$$

with

$$\frac{D}{Dt} = \frac{\partial}{\partial t} + \boldsymbol{U} \cdot \nabla \tag{2.45}$$

This is the convective derivative defined by the center-of-mass velocity unlike the separate fluid velocities which we used for the two-fluid model. If we assume an isotropic MHD pressure we can replace the tensor with a scalar pressure, P. The static equilibrium, Eq. (2.44) becomes:

$$\boldsymbol{I}_p \times \boldsymbol{B} = \nabla P \tag{2.46}$$

This equation describes the equilibrium between the magnetic pressure and tension, described by $\boldsymbol{I}_p \times \boldsymbol{B}$ and the total particle pressure, ∇P. The solution to this equation in two dimensions (an axi-symmetric cylindrical plasma) gives rise to the so called Bennett pinch or z-pinch. It was found that, theoretically, a small current could contain a considerable plasma pressure. However, these types of devices are highly unstable. Although Eq. (2.46) looks simple the solution in three dimensions is far from it. It can be written as a differential equation for the poloidal flux function ψ, and it has two arbitrary functions $p(\psi)$ and $F(\psi)$. The function $p(\psi)$ represent the particle pressure and the function $F(\psi)$ is related to

the combined poloidal current flowing in the plasma plus the toroidal field coils. A derivation can be found in [38] among others:

$$R^2\nabla\cdot\left(\frac{\nabla\psi}{R^2}\right) = -\mu_0 R^2\frac{dp}{d\psi} - \frac{1}{2}\frac{dF^2}{d\psi} \tag{2.47}$$

Here R is the major radius and μ_0 the magnetic permeability. From the solution for ψ the radial coordinate ρ_t, introduced in Chapter (2.2.1), can be determined. Numerical solutions of the equation describe the flux-surfaces and are used in simulation codes to describe the magnetic equilibrium. There are a number of analytical approximate solutions to the equation, one commonly used is the Miller model. The Miller model is an approximate description of each flux surface with nine parameters. These parameters describe different aspects of the magnetic equilibrium and many of these are crucial to confinement of the plasma. One of the most important is the safety factor q. The plasma current creates a poloidal magnetic field which makes the field line bend around the torus, the sharpness of the bend define the safety factor:

$$q = \frac{n_t}{n_p} = \frac{\langle \boldsymbol{B}\nabla\phi\rangle}{\langle \boldsymbol{B}\nabla\theta\rangle} \tag{2.48}$$

Here n_t is the number of toroidal turns compared to the number of poloidal turns n_p. The brackets denote flux surface averaging and the safety factor describes how twisted the magnetic fields are. It is a function of radial position and how rapid it changes is described by the magnetic shear.

$$\hat{s} = \frac{1}{q}\frac{\partial q}{\partial r} \tag{2.49}$$

Other important parameters are the aspect ratio ($\epsilon = r/R$), the elongation (κ) which describes the difference in length of the axis, triangularity (δ) which describes the shape of the flux-surface etc. An example of the Miller description can be seen in Figure (2.3) a) and the major radial dependence of the toroidal magnetic field, pressure and the magnetic current are shown in Figure (2.3) b).

2.6 Gyrokinetics

As mentioned in section (2.1), the charged particles are on average "bound" to a magnetic flux surface due to the Lorentz force. Hence it is sometimes more prudent to study the evolution of the the so called guiding-centers rather than the particles themselves. This can be taken a further step to the so called gyrocenter, as the guiding center still follows the particle true position, but with the guiding center as a reference. When handling gyrocenter the exact trajectory is of no interest and instead we follow the evolution of "charged rings". The quick gyromotion compared to the electromagnetic fluctuations is the basis of the so called gyrokinetic theory. By averaging out the fast gyromotion, the number of dimensions of the problem is reduced by one and a time step much greater than the gyroperiod is feasible. This is a great benefit in terms of reduced computational cost.

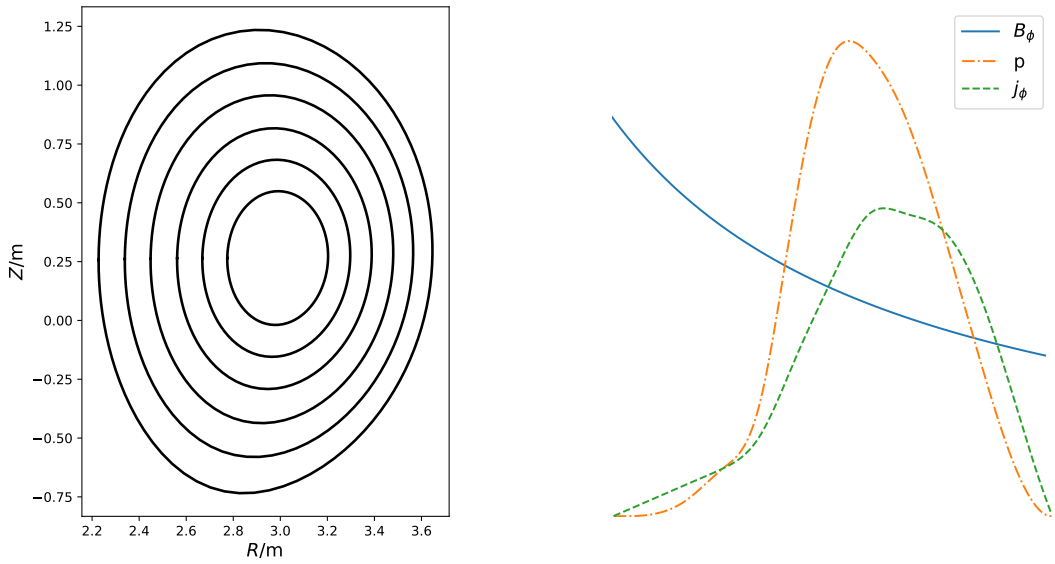

(a) Flux-surfaces

(b) B_ϕ, p and j_ϕ versus major R

Figure 2.3: Miller description of the flux surfaces. The figure to the right show the dependence of the major radial coordinate for the toroidal magnetic feld,B_ϕ, the toroidal current j_ϕ, and the plasma pressure, p

The modern derivation of the gyrokinetic theory is done by using canonical coordinate transformations which eventually result in equations of motion that are independent of the gyrophase angle. This derivation uses transformation first to the guiding-center and then to the gyrocenter by using Lie-formalism. A derivation can be found in [3]. Earlier derivations employed perturbation expansions and a direct gyrophase averaging. Both of these methods do however rely on the gyrokinetic ordering. The Larmor radius needs to be small in comparison to the scale length of the change in the background magnetic field, background densities and the background temperatures. The cyclotron frequency need to be much smaller than the frequency of turbulent fluctuations, $\omega/\omega_c \ll 1$. As the particles velocities along the magnetic field line are much greater than the drift velocities perpendicular to the fields, the spatial scales will be very different. The turbulence along the magnetic field lines are "stretched out" compared to the turbulence perpendicular which is comparable with the Larmor radius in scale. We can safely assume:$|\boldsymbol{k}_\parallel|/|\boldsymbol{k}_\perp| \ll 1$. We can summarize the gyrokinetic ordering:

$$\epsilon \sim \frac{\rho_i}{L_B} \sim \frac{\rho_i}{L_{n/T}} \sim \frac{\omega}{\omega_c} \sim \frac{e\delta\phi}{T} \sim \frac{|\boldsymbol{k}_\parallel|}{|\boldsymbol{k}_\perp|} \ll 1 \tag{2.50}$$

In gyrokinetic theory we do not study the evolution of the distribution in phase space, $\mathrm{f}(\boldsymbol{x}, \boldsymbol{v}, t)$, but instead the study the gyrocenter distribution function in gyrocenter phase space $\mathrm{F}(\boldsymbol{X}, v_\parallel, \mu)$. $\boldsymbol{X}$ is the gyrocenter position, $v_\parallel$ is the gyrocenter parallel velocity and μ is here again the magnetic moment, $\mu = mv_\perp^2/(2B)$. We

can rewrite the Vlasov equation, Eq. (2.24), in these coordinates:

$$\frac{\partial F}{\partial t} + \frac{d\boldsymbol{X}}{dt} \cdot \nabla F + \frac{dv_\parallel}{dt}\frac{\partial F}{\partial v_\parallel} + \frac{d\mu}{dt}\frac{\partial F}{\partial \mu} = 0 \tag{2.51}$$

The last term will disappear as the magnetic moment is constant. We decompose the electromagnetic fields into a background and a fluctuating part i.e. $\Phi \to \Phi_0 + \Phi_1$, $\boldsymbol{A} \to \boldsymbol{A}_0 + \boldsymbol{A}_1$. With this we can write the drift velocities for the gyrokinetic theory, here in Gaussian units.

- E x B drift
$$\boldsymbol{v}_\chi = -\frac{c}{B_0^2}\nabla\langle\Phi_1\rangle_{\boldsymbol{x}_{gc}} \times \boldsymbol{B}_0 \tag{2.52}$$
- ∇B-drift
$$\boldsymbol{v}_{\nabla B} = \frac{\mu}{m\omega_c}\hat{b} \times \nabla B_0 \tag{2.53}$$
- curvature drift
$$\boldsymbol{v}_c = \frac{v_\parallel^2}{\omega_c}(\nabla \times \hat{b})_\perp \tag{2.54}$$

Here again $\langle f\rangle_{\boldsymbol{x}_{gc}}$ denotes gyroaveraging. These velocity drifts are the equivalent of the drifts presented in Eq. (2.14). The fluctuating parts need to be much smaller than the background fields. We get the time derivative in these coordinates:

$$\frac{d\boldsymbol{X}}{dt} = v_\parallel\hat{b} + \frac{B_0}{B_{0\parallel}^*}(\boldsymbol{v}_\chi + \boldsymbol{v}_{\nabla B} + \boldsymbol{v}_c) \tag{2.55}$$

$$\frac{dv_\parallel}{dt} = -\left(\frac{\hat{b}}{m} + \frac{B_0}{mv_\parallel B_{0\parallel}^*}(\boldsymbol{v}_\chi + \boldsymbol{v}_{\nabla B} + \boldsymbol{v}_c)\right) \cdot \left(Ze\nabla\langle\Phi_1\rangle_{\boldsymbol{x}_{gc}} + \mu\nabla B_0\right) \tag{2.56}$$

$$\frac{d\mu}{dt} = 0 \tag{2.57}$$

Using all this we can write down the gyrokinetic Vlasov equation, here with σ denoting particle species:

$$\begin{aligned}&\frac{\partial F_\sigma}{\partial t} + \left(v_\parallel\hat{b} + \frac{B_0}{B_{0\parallel}^*}(\boldsymbol{v}_\chi + \boldsymbol{v}_{\nabla B} + \boldsymbol{v}_c)\right)\\ &\cdot\left(\nabla F_\sigma + \frac{1}{m_\sigma v_\parallel}\left(-Ze\nabla\langle\Phi_1\rangle_{\boldsymbol{x}_{gc}} - \mu\nabla B_0\right)\frac{\partial F_\sigma}{\partial v_\parallel}\right) = 0\end{aligned} \tag{2.58}$$

With $B_{0\parallel}^* = B_0 + \frac{B_0}{\omega_c}v_\parallel\hat{b}\cdot(\nabla\times\hat{b})$. In order to add collisions, we need to add a collision operator on the right hand side of the equation.

The distribution can be decomposed into a macroscopic part and a part describing the microturbulence with the assumption that the perturbed part is much smaller than the background, $F_\sigma \to F_{\sigma 0} + f_{\sigma 1}$. By using the gyrokinetic ordering to Eq. (2.58) to the zeroth order and decompose the distribution function we can see an interesting thing: The background distribution does not explicitly evolve in

time. This is used in δf-codes to choose a background distribution function which fulfills the zeroth order. As collisions drives the backgound distrubution towards a Maxwellian distrubution, this is the choice for gyrokinetic codes. GENE is a gyrokinetic code which uses the δf-approach [41].

In order to solve the gyrokinetic equation, a suitable coordinate system needs to be established. Before we embark onto that subject it is important to remind us that the many physical phenomena and structures in a plasma is highly anisotropic. The particles move along the magnetic field lines at high speed but move across them (due the drift velocities among other things) magnitudes slower. Hence the correlation length in the parallel direction is much longer than the perpendicular (this is also one of the assumption we used when introducing the gyrokinetic equation). This knowledge makes it possible to use different resolutions in different spatial coordinates and thus saving a large amount of computational cost. As we have a distinctive direction, which is the magnetic field, a coordinate system aligned to it is a natural construction. A good overview of flux coordinates can be found in [11]. To study the microturbulence for an entire present day tokamak, the required grid-size makes this simulation extremely expensive. These kind of simulations are done today on supercomputers but are rare. In order to systematically study a plasma phenomena the simulation domain is significantly reduced. This is done with the flux tube approximation. In this approximation a magnetic field is followed around the torus for a poloidal turn (for tokamaks, due to the axisymmetry). A curved and sheared box is created around this magnetic field. The magnetic geometry of this box is not calculated self-consistently with the turbulent fluctuations but is a numerical or an analytical solution to the Grad-Shafranov equation, Eq. (2.47). This box is of a small size compared to the size of the tokamak and the investigation of the plasma is therefore a local one for the flux tube approximation. Because it is a local investigation background quantities such as density and temperature as well as their radial gradients are kept constant throughout the box. This approximation is valid if the radial size of the box is small compared to the machine size but large enough compared to the microturbulence. The coordinate are x for the fluxlabel, i.e. the radial direction which is perpendicular to the flux surface, y is the binormal direction and z is the direction along the field line. As the flux tube approximation only covers a small part of the plasma we need to adapt proper boundary conditions which do not interfere with the physical phenomena which we want to study. In the radial and binormal coordinate periodic boundary conditions are a good choice.

$$F(x + L_x, y, z) = F(x, y, z) \ , \ F(x, y + L_y, z) = F(x, y, z) \tag{2.59}$$

Here L_x is the box size in the x direction and L_y is the box size in the y-direction. These boundary conditions also keep the number of particles and the energy conserved in the x and y direction. This ensure no accumulation of particles inside the simulation box. These periodic boundary conditions also ensure that we can make a Fourier representation in the two perpendicular directions. As the microinstabilities usually are localised at the bad curvature side (the low field side), the flux tube are joined at the high field (inner) side to create the boundary condition

in the parallel direction. Due to the helical magnetic field this boundary condition is more complex and beyond the scope of this thesis, for more detail see Ref. [44].

2.7 Gyrofluid

In the same manner as we got the fluid equations from the Boltzmann equation by taking moments we can get the gyrofluid equations from taking moments of the gyrokinetic equation, Eq. (2.58). The gyrofluid equations are equivalent to the fluid equations, Eq. (2.28), (2.32), and (2.35) and describe the evolution of the plasma. Thanks to the manner the gyrokinetic equation is derived, with the gyroaveraging, the gyrofluid approach has a number of gyroeffects that is not present in fluid descriptions of the plasma. Finite Larmor Radius (FLR) effects to all orders are naturally included in the gyrofluid equations, in the fluid models only first order FLR effects are usually included but higher order effects have been known to be added manually. FLR effects takes into account the average of fields over the fast gyration of a charged particle around the magnetic field that appears due to the small but non-zero size of the Larmor radius. Another phenomena is Landau damping which is included in the gyrofluid description through the closure used. Landau damping is the mechanism where a wave in the plasma lose (or gain) energy from interacting with particles. If the distribution function is monotonically decreasing with velocity, the plasma gains energy from the wave thereby damping the wave. For a description of taking velocity moments of the gyrokinetic equations see [37], among others.

CHAPTER 3

TURBULENT TRANSPORT

In order to make fusion an economically viable energy source, the fusion triple product, $n\tau_E T$, must be sufficiently large, where n is the particle density, τ_E is the energy confinement time and T is the temperature. The product was first introduced by John D. Lawson [43] and it is used to describe a lower limit for ignition of the plasma. An ignited plasma is self-sustained by the energy released in the fusion reactions. Unfortunately there are limitations for the density and temperature which limits the triple product. The density is limited by the Greenwald limit, which is an empirical stability condition and relates the averaged density to the plasma current: $\bar{n}/10^{20} = \kappa I_p$, where κ is the elongation and I_p is the plasma current in MA/m^3 [49]. The temperature (and density) are limited by the constrains on $\beta = \frac{nT}{B^2/2\mu_0}$ which describes the ratio between the plasma pressure and the magnetic pressure. If this values becomes too large, certain MHD instabilities will occur and disrupt the plasma. This limitation on the β is described by the Troyon Limit which accounts for the ballooning and kink mode-instabilities. The value of these constraints on the density and temperature can be shifted by creating a higher plasma current and stronger magnetic field. However, this is a challenging engineering problem. Another approach to increase the triple product is to improve the confinement time for the plasma. At the basic level, the diffusion (and confinement) in the plasma is determined by Coulomb collisions, which describes classical diffusion and has a step length comparable to the Larmor radius. Additions to this model were made in the 1960's when Galeev and Sagdev developed the neo-classical theory. This new theory incorporated the effects of the particle drifts from the non-uniform magnetic field which is inevitably in a torus shape. Neo-classical diffusion is much higher than classical diffusion has it has a step length of the width of banana orbits. The neo-classical theory suggested that the transport perpendicular to the flux surfaces were relativly small and made plasma physicists hopeful that in a matter of decades that fusion power would be on the electric grid. Unfortunately, this would not be the case. Neo-classical theory is successful at describing the transport along field lines, however perpendicular to the flux surface its magnitude is too low compared to experimental values. This new transport was named anomalous transport to emphasize its non-classical nature. Today, we know that the anomalous transport is caused

by microturbulence in the plasma. Small fluctuations of the densities, temperatures and electrostatic potential in the plasma might lead to turbulent transport. The study of the turbulent transport is the main goal of this thesis.

In this section we will describe turbulent transport. (I) First, we will describe the physical nature of the turbulence transport, the drift wave instabilities. (II) Second, we will discuss the difference between non-linear, linear and quasi-linear theory. (III) Third, we will describe linear theory in greater detail. (IV) Fourth, we will describe quasi-linear theory which is used to achieve fluxes from linear theory. (V) Fifth, we will discuss turbulent transport models and transport phenomena.

3.1 Drift Waves

Drift waves are an important type of microinstability which occur in the plasma owing to the free energy associate with the temperature and density gradients. A simple (but informative) ansatz for the transport coefficients is the mixing length estimate which gives the scaling for the effective diffusion:

$$D \sim \frac{\delta x^2}{\delta t} \sim \frac{\gamma}{k_\perp^2} \tag{3.1}$$

Here δx and δt is the step length in space and time, γ is the growth rate of the drift wave mode and $k_\perp$ is the associated wavenumber. This relation describes the spatial scale of an instability and determines the total amount of transport. A faster growing mode might not be as important as one with lower growthrate if its spatial scale is much smaller. This is true for the relation between the Ion Temperature Gradient (ITG)-mode and the Electron Temperature Gradient (ETG)-mode. These are equivalent but the ITG-mode is on ion Larmor scale and ETG-mode on electron Larmor scale, which means that the ITG-mode is (usually) much more significant. The nature and the origin of these instabilities will be discussed in the following sections.

The driftwave which is responsible for most of the turbulent transport in today's plasma experiments is the Ion Temperature Gradient (ITG) - mode. The ITG-mode is a Rayleigh–Taylor type instability which develops when a heavier fluid is on top a lighter one. The mode is associated with the free energy of the ion temperature gradient and the largest growthrate occurs at the spatial scale such that $k_y\rho_i \sim 0.3$ [32]. This is much smaller than the tokamak minor radius but large compared with the debye-length. Therefore the quasineutrality condition holds for the perturbed density associated with this mode, $\Sigma_j Z_j e\delta n_j = 0$, which we will use when discussing the origin of mode. The real frequencies of this mode is of the same magnitude as the diamagnetic or magnetic drift frequency.

The ITG-mode is formed by a series of physical events which creates a positive feedback loop. A simple way to describe the ITG -mode is to start with a small fluctuation in the ion temperature in the poloidal direction, δT_i. This leads to a difference in the magnetic drift velocity as it is dependent on the temperature, see Eq. (2.14). The different velocities leads to compression of the ion density in the poloidal direction, δn_i.

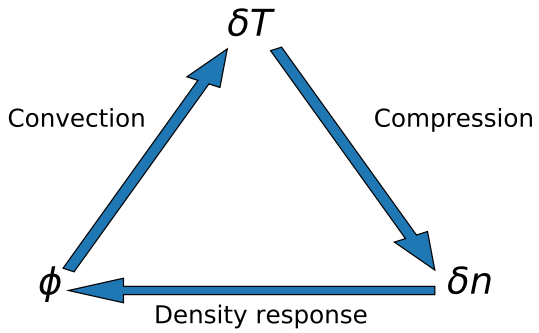

Figure 3.1: *Feedback loop for the ITG-mode*

This fluctuation in the ion density is followed by a fluctuation in the electron density as we assume the fluctuations follow quasineutrality. If we supposing Boltzmann distributed electrons (and for the time being ignore trapped electrons):

$$\delta n_e = n_e \frac{e\phi}{T_e} \tag{3.2}$$

The fluctuation in the electron density creates an electric field in the poloidal direction. The ExB drift, the first term in Eq. (2.14), is in the radial direction. If the background temperature gradient and magnetic field gradient are in the same direction (low field side), the ExB drift will increase the initial perturbations. In the opposite case when the background temperature gradient and magnetic field gradient are in the opposite direction (the high field side),drift will reduce the initial perturbations, essentially killing the instability. This is why the low field side is called the bad curvature region, which is where the largest fluctuations is encountered in the poloidal plane. The feedback-loop for the ITG-mode is displayed in Figure (3.1).

As the ITG-mode is such an important instability it has been extensively studied over the years. It has been shown both analytically and experimentally that there is a cut-off temperature-gradient [48], [31]. If the temperature gradient is sufficiently low the ITG-mode is stable.

Due to the higher magnetic field at the inner major radius electrons can be trapped at the outer, low field side of the torus. These particles do not travel around the whole torus but are trapped because of the magnetic mirror force if they do not have a high enough velocity parallel to the magnetic field. In order to have trapped electrons the collision frequency needs to be lower than the bounce frequency otherwise the collisions will scatter the particles before they can complete a bounce. As these electrons are trapped on the low field side the curvature drift, the middle term in Eq. (2.14), is not averaged out, as it is for a passing particle which travels to the high field side. This may give rise to the trapped Electron Mode or TEM. The trapped particles also give rise to the particle transport in the plasma, because for adiabatic electrons we do not get any particle transport and the trapped electrons make the total electron population non-adiabatic.

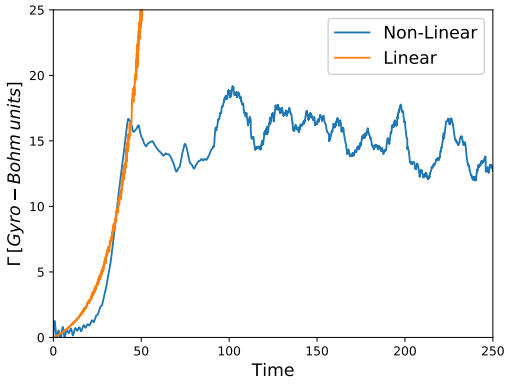

Figure 3.2: *The linear and non-linear phase of a gyrokinetic simulation of the DIII-D discharge 165303*

3.2 Linear, Quasi-Linear and Non-Linear modelling

The fluid and kinetic models, which we have described in Chapter (2), can be used in three distinctive ways: linear, quasi-linear or non-linear. The linear-,quasi- and non-linear simulations are different approaches to study the instabilities. In particular the quasi-linear model use results from linear simulations in combination with plasma parameters to calculate quantities such as fluxes. Linear models cannot account for the coupling between instabilities since it is a non-linear effect, however they are much faster to solve numerically. The easiest way to explain the difference between the linear and non-linear models is by looking at Figure (3.2) where we display the particle flux for a linear and non-linear simulation. The two simulations follow a similar pattern in the initial phase, both grows exponentially and the linear terms are much larger than the non-linear terms. However at a certain level the non-linear terms will become of the same magnitude as the linear terms and couplings between stable and unstable modes become important. This results in a saturated turbulent flux as can be seen in Figure (3.2) for the non-linear simulation. In the linear simulations the growthrate and the real frequency are the interesting results. For the non-linear simulation the fluxes are saturated beacuse of non-linear effects.

Quasi-linear theory assume linear relations, even in the non-linear stationary turbulent state, between the fields. The theory describes the connection between the growthrates, real frequencies and plasma parameters to the saturated fluxes. The saturation level have been derived analytically, which is described in Section (3.4), and by parameterisation of non-linear simulations. Even though theoretical understanding has helped derive quasi-linear expressions for the fluxes it is often necessary to compare and normalise with non-linear simulations to achieve good comparisons with experiments. As quasi-linear simulations are computationally much cheaper than non-linear simulations, they are ideal for integrated modeling. Hence, the development of quasi-linear models are important for the scientific community. In paper IV my co-authors and I improve the saturation model of the fluid model EDWM [32].

3.3 Linear theory

As previous mentioned, the Quasi-Linear models (or reduced models which they are sometimes called) calculate the turbulent transport from the linear response and the quasi-linear intensity, i.e. the saturation level for $|\phi|^2$. Different quasi-linear models have different linear response depending which physics is included. The quasi-linear intensity is determined by the linear instability, calculated from an dispersion relation and connected to the perturbed quantities using quasi-linear theory. QuaLiKiz [10] uses a gyro-kinetic dispersion relation, TGLF [17] a gyro-fluid dispersion relation and EDWM a fluid dispersion relation.

Here we will briefly discuss the derivation of a dispersion relation used in EDWM, in a simplified version. As it is a multi-fluid model it uses expressions from the moments of the Vlasov equation which we derived in Section (2.4). We here again express the continuity and heat flux equation.

$$\begin{aligned}
&\frac{\partial n_\sigma}{\partial t} + \nabla \cdot (n_\sigma \boldsymbol{u}_\sigma) = 0 \\
&\frac{3}{2} n_\sigma \left(\frac{\partial}{\partial t} + \boldsymbol{u}_\sigma \right) T_\sigma + n_\sigma T_\sigma \nabla \cdot \boldsymbol{u}_\sigma + \nabla \cdot \boldsymbol{Q} = 0 \\
&\boldsymbol{u}_\sigma = \boldsymbol{u}_E + \boldsymbol{u}_{\star,\sigma} + \boldsymbol{u}_{p,\sigma} + \boldsymbol{u}_{\pi,\sigma} + \hat{\boldsymbol{B}} u_{\parallel,\sigma}
\end{aligned} \tag{3.3}$$

The velocities are the drift velocities presented in Section (2.2) and they are as follow:

$$\begin{aligned}
\boldsymbol{u}_E &= \hat{\boldsymbol{B}} \times \nabla \phi / B \quad \textit{(ExB drift)} \\
\boldsymbol{u}_{\star,\sigma} &= \frac{\hat{\boldsymbol{B}} \times \nabla p_\sigma}{Z_\sigma e n_\sigma B} \quad \textit{(diagmagnetic drift)} \\
\boldsymbol{u}_{p,\sigma} &= \frac{d\boldsymbol{E}}{dt} / (B \omega_{c,\sigma}) \quad \textit{(polarization drift)} \\
\boldsymbol{u}_{\pi,\sigma} &= \frac{\hat{\boldsymbol{B}} \times \nabla \pi_\sigma}{Z_\sigma e n_\sigma B} \quad \textit{(stress tensor drift)}
\end{aligned} \tag{3.4}$$

In order to end up with the linear dispersion relation we need to linearize the equations, assuming a single Fourier harmonic, $f = f^{(0)}(r) + \delta f e^{i\boldsymbol{k}\cdot\boldsymbol{r} - i\omega t}$. Here, f represents density or temperature and the frequency is generally complex, $\omega = \omega_r + i\gamma$. ω_r is the real frequency of the mode and γ is the growthrate. A mode is unstable if $\gamma > 0$. The first part of f, represent the slow changing background value and the second term is perturbed part. In the proper derivation using a minimal number of assumptions which is used by EDWM we end up with a 10th order dispersion relation. This includes electromagnetic effects and parallel motion. We will make a simpler derivation which nonetheless is informative. The goal is to formulate the problem as an eigenvalue problem [45]. We make a couple of simplifications for our derivation, with $\widetilde{n} = \delta n e^{i\boldsymbol{k}\cdot\boldsymbol{r} - i\omega t}$

- $\nabla \widetilde{n}_\sigma / n_\sigma$ is assumed small as we are in the linear case
- Assume no background electric field, only perturbed

- Assume that the parallel motion term, $\nabla \cdot (n_\sigma \hat{\boldsymbol{B}} u_{\parallel,\sigma})$ is zero
- Assume electrostatic case

The continuity equation in Eq. (3.3) for the perturbed part of the density with these assumptions reduces to:

$$-i\omega\delta n_\sigma = -\nabla n_\sigma^{(0)} \cdot \delta \boldsymbol{u}_E - n_\sigma^{(0)} \nabla \cdot \delta \boldsymbol{u}_E + \underbrace{-\nabla \cdot [n_\sigma(\boldsymbol{u}_{p,\sigma} + \boldsymbol{u}_{\pi,\sigma})] - \nabla \cdot (n_\sigma \boldsymbol{u}_{\star,\sigma})}_{\text{Approximate to first order}} \quad (3.5)$$

The derivation of all terms on the right hand side is too long for convenience to display here. An derivation can be found in Appendix of [46]. The expressions are shown below:

$$\begin{aligned}
&-\nabla n_\sigma \cdot \delta \boldsymbol{u}_E = -\omega_{\star e} n_\sigma \frac{e\phi}{T_e} \\
&-n_\sigma \nabla \cdot \delta \boldsymbol{u}_E = -i\omega_{De} n_e \frac{e\phi}{T_e} \\
&-\nabla \cdot [n_\sigma(\boldsymbol{u}_{p,\sigma} + \boldsymbol{u}_{\pi,\sigma})] = i n_\sigma k^2 \rho_s^2 (\omega - \omega_{\star,\sigma T}) \frac{e\phi}{T_e} \\
&-\nabla \cdot (n_\sigma \boldsymbol{u}_{\star,\sigma}) = -\omega_{D,\sigma} \left(\delta n_\sigma + n_\sigma \frac{\omega}{\omega - 5\omega_{D,\sigma}/3} \left[\frac{2}{3} \frac{\delta n_\sigma}{n_\sigma} + \frac{\omega_{\star,e}}{\omega} \left(\eta_\sigma - \frac{2}{3} \right) \frac{e\phi}{T_e} \right] \right)
\end{aligned} \quad (3.6)$$

Here we introduced $\eta_\sigma = L_{n_\sigma}/L_{T_\sigma}$ and L_{n_σ/T_σ} is the gradient length for the density/temperature. We can use these terms in Eq. (3.5) and arrive at an expression for the ion density perturbation. Here times i/n_σ,

$$\begin{aligned}
&\frac{\delta n_\sigma}{n_\sigma} \left(\omega - \omega_{D,\sigma} - \frac{2}{3} \frac{\omega \omega_{D,\sigma}}{\omega - 5\omega_{D,\sigma}/3} \right) = \\
&= \frac{e\phi}{T_e} \left[k^2 \rho_s^2 (\omega - \omega_{\star,\sigma T} + \frac{\omega_{D,\sigma} \omega_{\star,e}}{\omega - 5\omega_{D,\sigma}/3} \left(\eta_\sigma - \frac{2}{3} \right) + \omega_{\star,e} - \omega_{D,e} \right]
\end{aligned} \quad (3.7)$$

We can get an expression for the normalizes perturbed density by multiplying with $\omega - 5\omega_{D,\sigma}/3$ and dividing with $N_\sigma = \omega^2 - 10\omega\omega_{D,\sigma}/3 + 5\omega_{D,\sigma}^2/3$

$$\begin{aligned}
&\frac{\delta n_\sigma}{n_\sigma} = \frac{e\phi}{T_e} \frac{1}{N_\sigma} \frac{1}{\varepsilon_n} \omega_{D,e}^2 \left[-\hat{\omega}^2 k^2 \rho_s^2 \varepsilon_n + \hat{\omega} \left(1 - \varepsilon_n - \frac{5}{3} k^2 \rho_s^2 \frac{\varepsilon_n}{\tau} - k^2 \rho_s^2 \frac{1 + \eta_i}{\tau} \right) + \right. \\
&\left. -\frac{1}{\tau} \left(\eta_\sigma - \frac{7}{3} + \frac{5}{3} \varepsilon_n \right) - k^2 \rho_s^2 \frac{5}{3\tau^2} (1 + \eta_\sigma) \right]
\end{aligned} \quad (3.8)$$

Here we have introduced the normalized frequency $\hat{\omega} = \omega/\omega_{D,e}$, normalized N $\hat{N}_\sigma = N/\omega_{D,e}^2$ and $\varepsilon_n = 2L_n/L_B$. A similar expression for the perturbed trapped electron density exists:

$$\frac{\delta n_{e,t}}{n_{e,t}} = \frac{e\phi}{T_e} \frac{1}{\hat{N}_e} \frac{1}{\varepsilon_n} \left[\hat{\omega}(1\varepsilon_n) + \left(\eta_e - \frac{7}{3} + \frac{5}{3} \varepsilon_n \right) \right] \quad (3.9)$$

The passing electrons are Boltzmann distributed as previously mentioned. The last step to derive this version of the linear dispersion relation is combining the perturbed densities in the quasi-neutrality condition:

$$\frac{\delta n_\sigma}{n_\sigma} - f_t \frac{\delta n_{e,t}}{n_{e,t}} - (1 - f_t)\frac{\delta n_{e,p}}{n_{e,p}} = 0 \tag{3.10}$$

Here f_t is the fraction trapped electrons. Using Eq. (3.8), Eq. (3.9) and the ratio for Boltzmann distributed electrons in this expression we end up with our dispersion relation:

$$\begin{aligned}
&\hat{N}_e \left[-\hat{\omega}^2 k^2 \rho_s^2 \varepsilon_n + \hat{\omega} \left(1 - \varepsilon_n - k^2 \rho_s^2 \frac{5}{3} \frac{\varepsilon_n}{\tau} - k^2 \rho_s^2 \frac{1 + \eta_\sigma}{\tau} \right) + \right. \\
&\left. -\frac{1}{\tau} \left(\eta_\sigma - \frac{7}{3} + \frac{5}{3} \varepsilon_n \right) - k^2 \rho_s^2 \frac{5}{3\tau^2} (1 + \eta_\sigma) \right] = \\
&= (1 - f_t) \hat{N}_\sigma \hat{N}_e \varepsilon_n + f_t \hat{N}_\sigma \left[\hat{\omega}(1 - \varepsilon_n) + \left(\eta_e - \frac{7}{3} + \frac{5}{3} \varepsilon_n \right) \right]
\end{aligned} \tag{3.11}$$

As $\hat{N}_\sigma$ and $\hat{N}_e$ includes ω squared this equation is a 4:th order linear dispersion relation. The proper expression for EDWM corresponds to a 10:th order dispersion relation when electromagnetic effects are included [32], for a plasma with one impurity species. The expression for $\hat{N}_\sigma$ and $\hat{N}_e$ are resonances and their relation determines in what direction the mode propagates, i.e. the sign of the real frequency. If $\hat{N}_\sigma < \hat{N}_e$ the mode moves in the ion direction, indicating an Ion Temperature Gradient (ITG) -mode. If $\hat{N}_\sigma > \hat{N}_e$ the mode moves in the ion direction, indicating a Trapped Electron -Mode (TEM). Eq. (3.11) can have both these modes unstable at the same time and the equation displays coupling between the modes. During resonance, i.e. $\hat{N}_\sigma = 0$ or $\hat{N}_e = 0$, the modes becomes decoupled and we get a pure ITG-mode or TEM.

We will now make the assumption, $\hat{N}_e << \hat{N}_\sigma$, which will result in a pure TEM. We will do this to be able to highlight the importance of critical temperature gradients. A critical gradient is where a mode becomes unstable, if a plasma has a temperature gradient lower than the critical, the associated mode is stable. These critical gradients are dependent on the plasma parameters. In our simplified version, the critical gradient will only depend on two plasma parameters. If we assume that $\hat{N}_e << \hat{N}_\sigma$ the LHS in Eq. (3.11) and if the solution has an imaginary part, it looks like:

$$\hat{\gamma} = \sqrt{\frac{f_t}{\varepsilon_n (1 - f_t)}} \sqrt{\eta_e - \eta_{cr}} \tag{3.12}$$

$$\eta_{cr} = \frac{9 f_t^2 + \varepsilon_n (24 f_t - 42 f_t^2) + \varepsilon_n^2 (40 - 80 f_t + 49 f_t^2)}{36 \varepsilon_n f_t (1 - f_t)} \tag{3.13}$$

To make the dependence on the temperature gradient clear we express these equations as temperature gradients. As $B \sim R^{-1}$ then $L_B = R$ and $\eta_e / \varepsilon_n = R / 2 L_{Te}$. We rewrite Eq. (3.12) and Eq. (3.13).

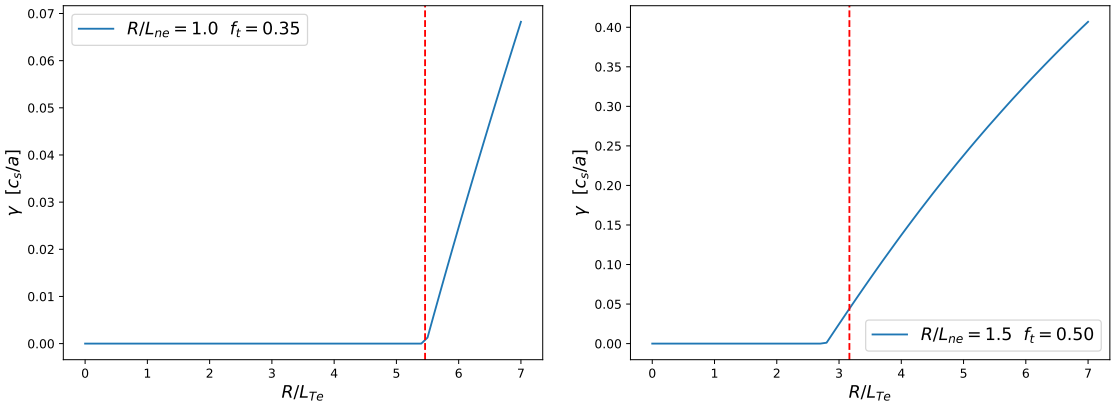

Figure 3.3: The growthrate for the TEM for an electron temperature gradient-scan with the fluid model EDWM. The dotted vertical line represent the theoretical critical gradient from our simplified equation which finds a similar value as EDWM. The left figure is the case with $R/L_{ne} = 1.0$ $f_t = 0.35$ and the right with $R/L_{ne} = 1.5$ $f_t = 0.50$.

$$\hat{\gamma} = \sqrt{\frac{f_t}{2(1-f_t)}}\sqrt{\frac{R}{L_{Te}} - \frac{R}{L_{cr}}} \tag{3.14}$$

$$\frac{R}{L_{cr}} = \frac{9f_t^2 + \frac{R}{L_{ne}}(24f_t - 42f_t^2) + \frac{R^2}{L_{ne}^2}(40 - 80f_t + 49f_t^2)}{18\frac{R^2}{L_{ne}^2}f_t(1-f_t)} \tag{3.15}$$

Eq. (3.14) makes it clear to have an instability the electron temperature gradient needs to be larger than the critical gradient. As previously mentioned this instability is the Trapped Electron Mode, hence we have a critical electron temperature gradient. We have calculated a couple critical gradients from Eq. (3.15) and compared them with simulations with EDWM. In Figure (3.3) we study the growthrate of the TEM over an electron temperature gradient scan. The dotted vertical line represent the value calculated by Eq. (3.15). We exemplify this for two cases: $R/L_{ne} = 1.0$ $f_t = 0.35$ (left) and $R/L_{ne} = 1.5$ $f_t = 0.50$ (right). We can notice in both cases that for low electron temperature gradient the mode is stable. At a certain gradient the growthrate becomes non-zero, this is where the mode is excited and thus the critical gradient of EDWM. In both figures in Figure (3.3) this occurs close to the value determined from our simplified equation implying even our simple model capture the physics in a satisfactorily way.

A critical gradient exist for the Ion Temperature Gradient in a similar fashion, here taken from [21] in the η - from.

$$\gamma = \frac{(\epsilon_n/\tau)^{1/2}}{1+k^2\rho_s^2}\omega_{*e}\sqrt{\eta_i - \eta_{i,th}} \tag{3.16}$$

$$\eta_{i,th} = \frac{1}{2}\left(\frac{4}{3} - \tau\right) + \frac{1}{4}\epsilon_n\left(\tau + \frac{40}{9\tau}\right) + \frac{\tau}{4\epsilon_n} \tag{3.17}$$
$$- \frac{k^2\rho^2}{2\epsilon_n}\left[\frac{5}{3} - \frac{\tau}{4} + \frac{\tau}{4\epsilon_n} - \left(\frac{10}{3} + \frac{\tau}{4} - \frac{10}{9\tau}\right)\epsilon_n + \left(\frac{5}{3} + \frac{\tau}{4} - \frac{10}{9\tau}\right)\epsilon_n^2\right]$$

As presented, linear theory solves the linear dispersion relation and determines the growthrate for each mode. However, to be able to calculate the fluxes due to the turbulence in the plasma we need to connect the growthrates, real frequency and other plasma parameters to the saturated quantities, such as the electrostatic potential which determines the fluxes. This is achieved by quasi-linear theory.

3.4 Quasi-linear theory

Quasi-linear theory connects the linear growthrates, real frequency and other plasma parameters to the saturated quantities, such as the electrostatic potential. The turbulent fluxes in the plasma are caused by the interaction between the electrostatic potential and the perturbed quantities (density, temperature). The turbulent fluxes are given by the linear phase difference between the perturbed quantities (density, temperature) and the ExB-drift.

$$\begin{aligned}\Gamma_i &= \langle \delta n_i v_{ExB}\rangle \\ Q_i &= \langle \delta T_i v_{ExB}\rangle\end{aligned} \tag{3.18}$$

here v_{ExB} is the ExB-drift velocity presented in Chapter (2) and δn the fluctuating part of the density. The brackets denote flux surface averaging. These parameters can be calculated numerically or can be expressed analytically to gain a better understanding of the transport. An analytical expression consist of two parts, a linear response (or quasilinear weight) and a quasi-linear intensity (or saturation level). The linear response govern the relation between the fluctuating part of the density, δn and the electrostatic potential ϕ. The quasilinear intensity describes the saturation of the electrostatic potential, which usually consist of a mixing-length assumption. The linear response is different for different models, here we present the expression for TGLF [8]:

$$\begin{aligned}\Gamma_i =& \Sigma_k \left\langle \frac{k_y c_s^2}{\omega_{ci}} \int F_M \frac{(\hat{\gamma}_k + \hat{\nu}_k)[R/L_{\langle n\rangle} + (E/T_e - 3/2)R/L_{\langle T_e\rangle}] - (\hat{\gamma}_k\hat{\omega}_{Gk} + \hat{\omega}_{rk}\hat{\nu}_k)}{(\hat{\omega}_{rk} + \hat{\omega}_{Gk})^2 + (\hat{\gamma}_k + \hat{\nu}_k)^2} \right. \\ & \left. \times J_0(k_\perp\rho_s)^2 |\hat{\phi}|_k^2 \right\rangle\end{aligned} \tag{3.19}$$

Where γ is the growthrate of the mode and k_y is the associated wave number. $\hat{\nu}_k$ is the collision-frequency, F_M is the equilibrium Maxwellian distribution function and all quantities with a hat in Eq. (3.19) are normalized with the

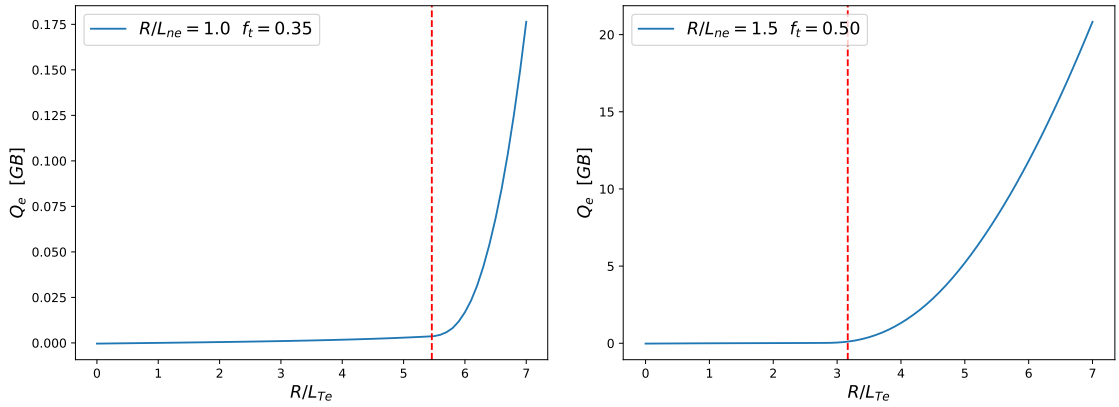

Figure 3.4: Electron heat flux for the TEM for an electron temperature gradient-scan with the fluid model EDWM. The dotted vertical line represent the theoretical critical gradient from our simplified equation which finds a similar value as EDWM. The fluxes increase rapidly after the critical gradient. The left figure is the case with $R/L_{ne} = 1.0$ $f_t = 0.35$ and the right with $R/L_{ne} = 1.5$ $f_t = 0.50$.

fluid perpendicular drift frequency, $\omega_{Dk} = k_y \rho_s c_s / R$. We have introduced the gradient length: $L_{\langle X_e \rangle} := -\left(\langle |\boldsymbol{\nabla} \rho_t| \rangle \frac{\partial}{\partial \rho_t} \ln \langle X_e \rangle \right)^{-1}$. The brackets denote flux surface averaging.

The sum is over all wavenumbers but only a limited part of the spectrum at low wavenumber has a significant contribution to the fluxes as discussed later. The last part of Eq. (3.19) describes the saturation level, also called quasi linear intensity, which is discussed later in detail. It is clear that it is essential that the linear phase differences calculated by turbulent transport models have similar values as the non-linear counterpart. This is one of the two main criteria for quasi-linear theory. This criteria has been extensively studied by comparing non-linear and quasi-linear simulations and generally holds [6] [15]. Secondly, the random walk assumption need to hold and a condition for this is that the Kubo number [42] needs to be smaller than 1. The Kubo number represent the ratio between the decorrelation time for the electrostatic potential and the turbulent eddy turn over time. The Kubo number has been calculated for several plasmas in different machines and different turbulence regimes and it has consistently been lower than 1 [7] [26]. Hence, it has been shown that for typical plasma parameters the random walk assumption is valid.

The output from quasi-linear models are the fluxes but they are deeply influenced by the growthrate from the instabilities in the plasma. This is made clear by the comparison of Figure (3.3) and Figure (3.4). Again, Figure (3.3) displays the growthrate from EDWM for a electron temperate gradient scan and Figure (3.4) display the electron heat flux for the same simulations. If the mode is not unstable it does not contribute to the fluxes which is why we have no flux when the growthrate is zero. As the growthrate becomes larger, the fluxes follow suit.

The value of critical gradient is crucial for the profiles in the plasma. When the mode is excited a small increase can lead to a massive increase in the

fluxes, which is most easily seen in Figure (3.4) (left). This means even a larger input of (additional) heating might not change the profiles in a significant way. This phenomena is described as the profile stiffness. They do not react to a large change in input heating.

3.4.1 Mixing length assumption

The connection between the electrostatic potential and the linear growthrate is expressed by the mixing length assumption which will result in an expression for the saturation level, the last part in Eq. (3.19). It is derived by assuming the convective ExB non linearity in the energy equation is balanced by the linear growthrate:

$$\gamma \delta T_j \sim \boldsymbol{v}_{ExB} \cdot \nabla \delta T_j \tag{3.20}$$

A similar expression for the perturbed part of the density exists which gives the same saturation level. One approach for the mixing length is to assume that the relevant physics occur at certain correlation length scales, described by $k_{x,a}$ and $k_{y,a}$ and use it in Eq. (3.20). The correlation length is the typical length scale for the turbulent transport where we have the highest transport and (a) indicates the wavenumbers at this length scale. We end up with the mixing length assumption which may be written as:

$$\frac{e\phi_a}{T_e} = \hat{\phi_a} = \frac{\gamma}{k_{x,a}k_{y,a}} \frac{1}{\rho_s c_s} \tag{3.21}$$

In principle this equation is only valid for $k_{x,a}$ and $k_{y,a}$, hence only for a quasi-linear model which uses a single poloidal wavenumber, such as the Weiland model. An improved treatment of the mixing length can be found by looking more thoroughly at Eq. (3.20). The gradients in the ExB-drift velocity and of the perturbed quantities are easily calculated if we express them and the electrostatic potential as Fourier series. Here for a slab geometry with x as the radial coordinate and y the poloidal.

$$\begin{aligned} \delta T(x,y) &= \sum_{k_{x1},k_{y1}} \delta T_{k_{x1},k_{y1}} e^{ik_{x1}x} e^{ik_{y1}y} \\ \phi(x,y) &= \sum_{k_{x2},k_{y2}} \phi_{k_{x2},k_{y2}} e^{ik_{x2}x} e^{ik_{y2}y} \end{aligned} \tag{3.22}$$

here, $\delta T_{k_{x1},k_{y1}}$ and $\phi_{k_{x2},k_{y2}}$ are Fourier coefficients and are independent of the spatial coordinates. The RHS of Eq. (3.20) becomes:

$$\sum_{\substack{k_{x1},k_{y1} \\ k_{x2},k_{y2}}} \left(\frac{k_{x1}k_{y2}}{B} - \frac{k_{x2}k_{y1}}{B} \right) \delta T_{k_{x1},k_{y1}} \phi_{k_{x2},k_{y2}} e^{ix(k_{x1}+k_{x2})} e^{iy(k_{y1}+k_{y2})} \tag{3.23}$$

We notice that we get two similar terms, one from the radial direction and one from the poloidal from the inner product in Eq. (3.20). We can remove

the spatial dependency by multiplying with test functions $e^{ik_{x3}}$ and $e^{ik_{y3}}$, thereafter integrating over the slab-geometry. We end up with an expression:

$$\gamma_{k_{x3},k_{y3}}\delta T_{k_{x3},k_{y3}} \sim \sum_{k_{x2},k_{y2}} \left(\frac{k_{x3}k_{y2}-k_{x2}k_{y3}}{B}\right)\delta T_{k_{x3}-k_{x2},k_{y3}-k_{y2}}\phi_{k_{x2},k_{y2}} \tag{3.24}$$

This equation express the balance between the linear growth and the non-linear mode coupling. The linear term for each poloidal wavenumber is balanced by a sum over wavenumber for the non-linear interaction term. This summation is referred as the Drift Wave Mixing. The expression for the mixing length, Eq. (3.21), express the same physics as Eq. (3.24), although in a more rudimentary version. The mode-coupling in Eq. (3.24) can not properly be represented in a quasi-linear model and as the Eq. (3.21) is only valid at the correlation length. An approach to circumvent this conundrum is presented in Paper IV: We propose that the saturation level is taken at the correlation length scale and all dependence of the poloidal wavenumber is contained in a filter *f*, representing the mode-coupling. We write the electrostatic potential as:

$$|\hat{\phi}|^2 = \frac{4\gamma_a^2}{\omega_{Dea}R^2k_a^2}f^2(k_y) \tag{3.25}$$

Here normalized with ω_{De}, the electron diamagnetic drift frequency. The fraction is calculated at the correlation length and the function f determines the spectral shape. Paper IV determines the spectral filter for the fluid model EDWM. With an expression for electrostatic potential we can use Eq. (3.19) to determine the fluxes form the turbulent transport.

3.5 Transport modeling

In this section we are presenting the models which have been used in the papers.

3.5.1 EDWM

EDWM (Extended Drift Wave Model) is based on the Weiland model created at Chalmers University of Technology in the 90s [48] and it is applicable for turbulent transport in conventional tokamaks. It is a fluid model which was initially developed only for the Ion Temperature Gradient mode [21] and subsequently expanded to include the Trapped Electron-Mode [22]. EDWM only considers instabilities at ion scales and does not include instabilities at smaller scales, such as the Electron Temperature Gradient (ETG)-mode. EDWM can handle an arbitrary number of ions and all their possible charge states [28]. Higher order Finite Larmor Radius-effects has been added to the later version of EDWM. The derivation of the multi fluid model starts with the Braginskii equations coupled to Maxwells equations. It is electromagnetic and as a consequence, the free electrons are not Boltzmann distributed due to the correction from the vector potential parallel with the magnetic

field. Another electromagnetic effect is the stabilization of the Ion Temperature Gradient (ITG)-mode, which usually is the dominant turbulent instability in current experimental devices. EDWM uses a toroidal slab geometry and the ExB-shearing rate is taken into account as a reduction in the linear growth rate in the Hahm-Burell formalism [39]. As EDWM uses an eigenvalue solver, all unstable modes not just the most unstable, account for the total flux.

3.5.2 TGLF

The Trapped-Gyro Landau-Fluid model or TGLF [17] for short includes effects that are not present in the fluid models. Landau damping and Finite Larmor Effects are not added in fluid models accurately. TGLF uses Miller geometry [34] and includes electromagnetic effects. TGLF is a quasi-linear model which by taking moments of the gyrokinetic equations, as described in Sec. (2.7), results in a set of coupled equations. These equations are solved for the linear eigenmodes of the ion and electron temperature gradient (ITG,ETG), trapped ions and electrones modes (TI, TE) and electromagnetic balloning mode (KB modes). A wide spectrum is used for the wavelengths, including both ion scales ($k_\theta \rho_s < 1$) and electron scales ($1 < k_\theta \rho_s < 24$). The saturation level for the TGLF is fitted to a database of nonlinear gyrokinetic simulations. The saturation used in the papers are SAT1 [19, 18].

3.5.3 GENE

The GENE-model uses a Eulerian δf-method to solve the nonlinear gyrokinetic Vlasov equation [41]. GENE solves for the fluctuating part of the distribution function $\delta f(\mathbf{R}, v_\parallel, \mu, t)$, the parallel component of the vector potential, $A_\parallel(\mathbf{x}, t)$, the parallel component of the magnetic field perturbations, $B_\parallel(\mathbf{x}, t)$ and the electrostatic potential $\phi(\mathbf{x}, t)$. The model uses a magnetic field aligned flux coordinate system where x is aligned to the radial coordinate, y the binormal coordinate and z parallel to the magnetic field and it can handle an arbitrary number of ion species. We have used the linearized Landau-Boltzmann operator [44] for the collisionality and in the papers we used a realistic geometry geometry by using an EFIT-file to calculate the magnetic equilibrium.

3.5.4 Integrated modeling

In the previous section we discussed specific turbulent transport models which uses plasma parameters and calculate the particle fluxes, heat fluxes, growthrates of the modes etc. These codes can be used together with other models, such as for heating, magnetic equilibrium, neoclassical transport, to simulate the whole plasma, this is called integrated modeling. Integrated modeling can be used in two ways, interpretative and predictive modeling. Interpretative modeling uses given plasma profiles as input to the codes and calculates a number of different quantities such as, particle deposition, linear growth rates, particle fluxes etc. Predictive simulations evolve the plasma profiles (n, T, J, v_{tor}) in time, self-consistently.

One integrated model which have been used in Paper A, B and C is the JETTO-code [4]. Experimental profiles are taken from quasi-steady state, where the outward fluxes are in balance with the internal sources, as a starting point and the predictive simulations are evolved in time until they find the theoretical quasi-steady-state. These theoretical quasi-stedy states are compared with the experimental (physical) steady state to asses the validity of the theoretical models. With integrated modeling it is feasible to determine the response of the plasma due to external changes (for example increase of the NBI particle source). During the evaluation of the plasma profiles the turbulent transport models are consistently calculated as they are significantly affected by changes in the profiles.JETTO performs these predictive simulations by solving the particle (i.e. continuity) and energy balance equations and evolving it in time. Here as flux surface averaged equations [4]:

$$\frac{\partial}{\partial t}\langle n\rangle + \frac{1}{v'}\frac{\partial}{\partial \rho_t}\left(v'\langle \Gamma^{\rho_t}\rangle\right) = \langle S_n\rangle \tag{3.26}$$

$$\frac{3}{2}\frac{\partial\langle P_j\rangle}{\partial t} + \frac{1}{v'}\frac{\partial}{\partial \rho_t}\left[v'\langle \boldsymbol{q}_i \cdot \boldsymbol{\nabla}\rho_t\rangle\right] = \langle Q_j\rangle \tag{3.27}$$

S_n is the NBI particle source and Q represent the power gain and losses from NBI-particles, electron-ion thermal equilibration, radiation and Ohmic heating. Both S_n and Q is dependent on the radial position and both can be calculated with various degree of accuracy. It is preferable to calculate the source profiles several times during a simulation as changes in the profiles affect the deposition of the sources.

3.6 Turbulent transport phenomena

In this section we discuss some turbulent transport phenomena which is discussed in greater detail in the articles.

3.6.1 Density Peaking

Because the densities are constrained by the empirical Greenwald limit, which mainly limits the density at the plasma edge, in order to achieve high fusion power it is favorable to have a peaked density profile.

The density peaking is determined by two factors, the particle sources and the particle transport. Previous work have studied the importance of the particle sources for the density peaking, and the results are inconclusive. Some studies have shown the particle sources to have a high impact [30, 20] while others have shown a low (around 20 % of the density peaking from the particle sources) or negligible impact [23, 29, 8]. Furthermore, more recent studies at JET [36, 14] showed that the particle sources had a large effect on the peaking while other studies at DIII-D [35] and AUG [13] showed a small or negligible contribution from the particle sources. Because the density peaking is important for the effectiveness of a future power plant, it is imperative to clarify the relative contributions from the particle

sources and transport to the density peaking. Density peaking can be defined in two different ways, global or local. Global density peaking describes the normalized density difference between the core and the top of the H-mode pedestal. Local density peaking is defined by the normalized density gradient at a certain radial position in the plasma. In this thesis the focus is on the local density peaking and its origins.

In order to discuss density peaking properly we need to introduce the concept of diffusion and pinch. If we look at Eq. (3.19) we notice that the expression is divided into three specific parts. We have one part which is explicitly proportional to the density gradient, this is the diffusive part and it is directed outwards. A second term explicitly proportional to the temperature gradient and it is called the thermo-diffusion pinch. The last part is not explicitly dependent on any of the gradients of the density or temperature and is the convective pinch. Both the pinch terms can be directed inwards or outwards. The thermo-diffusion and the convective pinch can be added together which we will do from here on. From these concepts we can define a decomposed particle flux of a diffusive and pinch part, here in a non-circular geometry as we included the metric components $\langle|\boldsymbol{\nabla}\rho_t|\rangle$ and $\langle|\boldsymbol{\nabla}\rho_t|^2\rangle$. (for details see Paper III)

$$\langle\Gamma_e^{\rho_t}\rangle = -D^{PB}_{\langle n_e\rangle}\langle|\boldsymbol{\nabla}\rho_t|^2\rangle\partial_{\rho_t}\langle n_e\rangle + V^{PB}_{\langle n_e\rangle}\langle|\boldsymbol{\nabla}\rho_t|\rangle\langle n_e\rangle \tag{3.28}$$

Here $\partial_{\rho_t} = \partial/\partial\rho_t$, $D^{PB}_{\langle n_e\rangle}$ is the diffusion and $V^{PB}_{\langle n_e\rangle}$ is the pinch. To quantify local density peaking we will start with the flux surface averaged continuity equation from (3.26):

$$\frac{\partial}{\partial t}\langle n\rangle + \frac{1}{v'}\frac{\partial}{\partial\rho_t}\left(v'\langle\Gamma^{\rho_t}\rangle\right) = \langle S_n\rangle \tag{3.29}$$

Here Γ is the particle flux shown in Eq. (3.28). The density peaking has two sources, the turbulent transport and the particle source due to the Neutral Beam Injection. This can clearly be seen by inserting the decomposed particle flux in Eq. (3.29) and assume quasi steady-state.

$$\frac{a}{L_{\langle n_e\rangle}} = -\frac{a\langle|\boldsymbol{\nabla}\rho_t|\rangle^2}{\langle|\boldsymbol{\nabla}\rho_t|^2\rangle}\frac{V^{PB}_{\langle n_e\rangle}}{D^{PB}_{\langle n_e\rangle}} + \frac{a\langle|\boldsymbol{\nabla}\rho_t|\rangle}{v'\langle|\boldsymbol{\nabla}\rho_t|^2\rangle\langle n_e\rangle D^{PB}_{\langle n_e\rangle}}\int_0^{\rho_t} v'\langle S_n\rangle d\rho_t \tag{3.30}$$

Here v' is the the derivative of the plasma volume, $\langle S_n\rangle$ is the particle input from the particle source per flux surface/s. The left hand side is the total local peaking factor for the plasma. The first term on the RHS is the peaking that comes from the turbulent transport. This term is entirely determined by the ratio of the particle balance pinch and diffusion. The second term on the right hand side is the source term and reduces as the particle balance diffusion increases. A discharge with high particle balance diffusion can still be peaked through the turbulent transport, if the particle balance pinch is of the same magnitude as the diffusion or stornger.

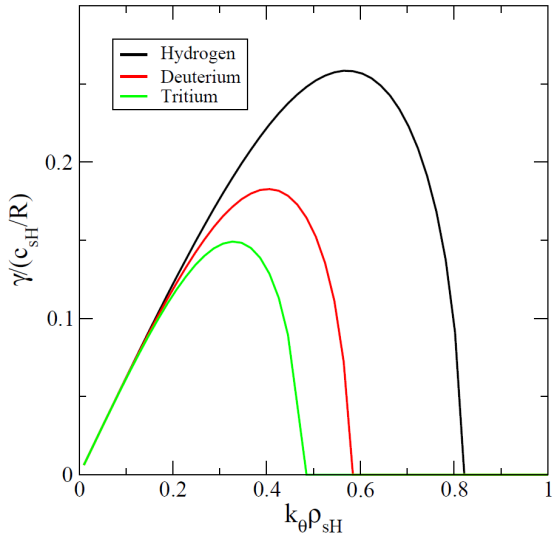

Figure 3.5: *Growhrates for different isotopes, all normalized with hydrogen. Taken from [32], with permission.*

3.6.2 Isotope effect

The isotope mass affects the turbulent transport in the plasma in several ways. Heavier elements have a larger gyro-radius ($\rho_L \propto \sqrt{M}$) for the same charge and as the gyro-radius is closely linked to the scale of the turbulence. The effect of the gyro-radius on the ITG growth rate is displayed in Figure (3.5) which show the growth rates for the different isotopes. Because the tritium is the heaviest isotope it has the largest scale for its turbulent, i.e. lowest wave number, and hydrogen the smallest scale, i.e. highest wave number. We can also notice the difference in the maximum value of growth rates which decreases for heavier isotopes. These two effects, different scale and different growthrates, are dependent of the mass in the same way, $k_{max} \propto M^{-0.5}$, $\gamma \propto M^{-0.5}$. This to effects combined make the turbulent flux scale with mass as $\Gamma \propto \gamma/k^2 \propto \sqrt{M}$ as presented Eq. (3.1). However, this is not that is generally observed experimentally. This discrepancy is referred the "isotope effect".

Experimentally studies have shown that global stored energy scale as $M^{0.2}$ for a multi-machine database [25]. A key factor that could alter the scaling was first proposed by Cordey et al [5], who observed that the core and the edge transport in the plasma can be very different, i.e. it is not necessary that transport in the edge scale in the same way as in the core. For instance, it is possible the imagine that core transport is gyro-Bohm like while the global stored energy scales with a positive exponent of M because of the edge pedestal. Experimentally, it has been well established in several devices that the edge plasma in a tokamak H-mode has a strong dependency on the isotope, e.g. in JET [27], AUG [33], JT-60U [47] etc. In a recent regression analysis of a large JET (ILW) pedestal database, a significant dependency was found for the pedestal stored energy, $\propto M^{0.5}$ [27], where both the density and temperature at the top of the pedestal where found to increase with isotope mass. An increased pedestal should usually lower the normalized gradient

and thereby lower the turbulent transport. Hence, what is perceived as an anti-gyro Bohm effect in the core turbulent transport may be caused by the change in pedestal.

There are plenty of mechanism that could break the gyro-Bohm dependence for the turbulent transport in the core. These includes (i) collisions [9]; (ii) ExB shear [24], [12], (iii) β-effects and contribution of the Electron Temperature Gradient (ETG) mode. The isotope effect is explored in some detail for JET dsicharges in Paper V.

CHAPTER 4

BRIEF SUMMARY OF THE PAPERS

The common feature through papers I-III is the assessment of the relative importance of the particle source for the density peaking in current tokamak devices with the aim of improving the extrapolation to future machines. Paper IV focuses on the development of the saturation rule in the fluid model EDWM and Paper V studies the isotope effect for three JET H-mode discharges.

In Paper I, interpretative and predictive simulations with JETTO for four collisionality scans at JET are presented each with three discharges: Deuterium L-mode with Carbon wall, hydrogen H-mode with Iter Like Wall (ILW), deuterium H-mode with ILW and deuterium H-mode with high β and ILW. In the predictive simulations, the electron density, electron and ion temperature profiles were evolved until a quasi-steady state was found. In each collisionality scan, important dimensionless parameters were kept constant such as β, normalized gyro-radius, safety factor, magnetic shear, normalized temperature gradients and Z_{eff}. To identify the effect of the NBI-source on the density peaking, simulations were performed with the NBI particle source and in a second case were it was artificially removed while maintaining the power input from the NBI. The simulations were carried out with JETTO using TGLF as transport model. The results showed that the turbulent pinch was the major cause of the density peaking for the L-mode discharges while the H-mode discharges showed a strong dependency on the NBI-source. As discharges with carbon wall has a higher impurity content these discharges were also simulated with a 2% carbon content which did not affect the density peaking in a significant way. The TGLF model predicts the experimentally profiles relatively well.

In Paper II, a collisionality scan performed at DIII-D was studied. The perturbative transport coefficients were measured using a gas puffing techniques and results showed larger values for these coefficients for the low collisionality discharge, both for the diffusion and pinch coefficients. The ratio of the two transport coefficients represents the turbulent transport contribution to the density peaking. The calculated ratios were close to the measured density peaking indicating that the NBI fueling had a small impact on the peaking. Studies were done with TGLF to determine the linear stability properties. The medium and high collisionality discharges

had a dominant ITG-mode and the low collisionality discharge displayed a TEM as the most unstable mode which might explain the large difference in transport coefficients.

In Paper III is focused on the comparison of the particle transport and density peaking between JET and DIII-D. This was done by comparing two H-mode collisionality scans, one at JET and one at DIII-D. The perturbative particle transport coefficients were calculated by performing density gradient scans for the discharges with TGLF. Particle balance transport coefficients were also calculated and where found to be lower than the perturbative values which suggest that one generally can not make the assumption that the perturbative and particle balance transport coefficients are equal. The ratio between between the particle balance pinch and diffusion coefficients were calculated since its values represent the turbulent transport contribution to the density peaking. Results showed that in the DIII-D discharges the majority of the density peaking was due to the turbulent transport while the JET discharges had strong contribution from the particle source. This conclusion was also supported by linear and non-linear GENE simulations. Sensitivity studies were performed to determine which parameters were responsible for the large difference in the contribution to the density peaking in DIII-D and JET. The largest effect came from the differennce temperature gradients.

In Paper IV, we focus on enhancing the physics fidelity of the quasi-linear fluid model EDWM (Extended Drift Wave Model). We have developed a new saturation model and calibrated several other features. As one of the computationally fastest first-principle based core transport models, EDWM can include an arbitrary number of ions and charge states. This feature is especially important for experimental devices with plasma facing components made of heavy elements, such as JET and the upcoming ITER-device. Because EDWM is a quasi-linear model it solves a linear dispersion relation to obtain the instabilities driving the turbulence. Furthermore, it combines the linear description with an estimation of the saturation level of the electrostatic potential. A new saturation rule at the characteristic wavenumber combined with a spectral filter for the poloidal wavenumber dependency were developed. The shape of the filter has been adapted to the poloidal wavenumber spectra obtained from non-linear gyrokinetic simulations. Additionally, EDWMs collision frequency and safety factor dependencies, as well as the electron heat flux level have been calibrated against gyrokinetic and gyrofluid results. Finally, the saturation level of the turbulence has been normalized against non-linear gyrokinetic simulations and later validated against experimental measured fluxes from 12 discharges at JET.

In Paper V, we studied the isotope effect in three discharges at the Joint European Torus (JET). The term isotope effect is used to label the deviation between experimental measurements and the simple gyro-Bohm scaling. The latter postulates that the stored energy in the plasma scale as $1/M_{eff}^{1/2}$, where M_{eff} is the effective mass of the fuel isotope(s). This phenomena has received considerable attention in recent years. However, a complete understanding of the deviation from gyro-Bohm scaling is still lacking. The plasma species used in the JET experiments were a mixture of hydrogen and deuterium, M_{eff} varying between 1 and 2. The discharges were matched in terms of engineering parameters, with a plasma current

of 2.3 MA, a magnetic field of 2.3 T and Neutral Beam Injection (NBI) heating power of 22 MW. We have analysed the discharges with linear and non-linear gyrokinetic simulations as well as with the integrated modelling framework ETS. In particular, the analysis was concentrated on four effects that could lead to a deviation from gyro-Bohm scaling of the core confinement: (i) the "boundary condition" presented by the H-mode pedestal for the core confinement; (ii) $\boldsymbol{E} \times \boldsymbol{B}$ shearing because of the external rotation induced by Neutral Beam Injection; (iii) collisions; and (iv) contribution of Electron Temperature Gradient modes (ETG modes) to the plasma transport. It was found that the first two make the main contribution to the deviation of the core confinement from gyro-Bohm scaling in the analysed JET discharges.

BIBLIOGRAPHY

[1] P. Bellan. *Fundamentals of Plasma Physics*. Cambridge University Press.

[2] I. Braginskii. *Reviews of Plasma Physics 1*. Consultants Bureau, 1965.

[3] A.J. Brizard and T.S. Hahm. Foundations of nonlinear gyrokinetic theory. *Reviews of modern physics*, 79, 2007.

[4] G. Cennachi and A. Taroni. Jetto: Tech. rep. jet-ir (88) 03 jet reports. 1988.

[5] J.G. Cordey. H mode power threshold and confinement in jet h, d, dt and t plasmas. *Nucl. Fusion*, 39(1763), 1999.

[6] T. Dannert and F. Jenko. Gyrokinetic simulation of collisionless trapped-electron mode turbulence. *Phys. Plasmas*, 12(072309), 2005.

[7] A. Casati et al. Validating a quasi-linear transport model versus nonlinear simulations. *Nucl. Fusion*, 49(085012), 2009.

[8] C. Angioni et al. Particle transport in tokamak plasmas, theory and experiment. *Plasma Phys. Control. Fusion*, 51(124017), 2009.

[9] C. Angioni et al. Dependence of the turbulent particle flux on hydrogen isotopes induced by collisionality. *Phys. Plasmas*, 25(082517), 2018.

[10] C. Bourdelle et al. A new gyrokinetic quasilinear transport model applied to particle transport in tokamak plasmas. *Phys. Plasmas*, 14(112501), 2007.

[11] D'haeseleer, W.D. et. al. *Flux Coordinats and Magnetic Field Structure*. Springer Series in Computational Physics.

[12] D.R. Ernst et al. Unifying role of radial electric field shear in the confinement trends of tftr supershot plasmas. *Physical Review Letters*, 81(21), 1998.

[13] E. Fable et al. The role of the source versus the collisionality in predicting a reactor density profile as observed on asdex upgrade discharges. *Nucl. Fusion*, 59(076042), 2019.

[14] F. Eriksson et al. Interpretative and predictive modelling of jet collisionality scans. *Plasma Phys. Control. Fusion*, 61(102487), 2019.

[15] F. Jenko et al. Heat and particle transport in a tokamak: advances in nonlinear gyrokinetics. *Plasma Phys. Control. Fusion*, 47(B195-B206), 2005.

[16] G. Bateman et al. Effect of isotope mass on transport simulations of joint european torus highmode plasmas with edge localized modes. *Phys. Plasmas*, 67(4607), 1999.

[17] G. Staebler et. al. Gyro-landau fluid equations for trapped and passing particles. *Phys. Plasmas*, 12(102508), 2005.

[18] G. Staebler et. al. The role of zonal flows in the saturation of multi-scale gyrokinetic turbulence. *Phys. Plasmas*, 23(062518), 2016.

[19] G. Staebler et. al. A model of the saturation of coupled electron and ion scale gyrokinetic turbulence. *Nucl. Fusion*, 57(066046), 2017.

[20] Garzotti, L. et al. Simulations of source and anomalous pinch effects on the density profile peaking of jet h-mode plasmas. *Nucl. Fusion*, 46(994), 2006.

[21] H. Nordman et al. Transport due to toroidal η_i mode turbulence in tokamaks. *Nucl. Fusion*, 29(251), 1989.

[22] H. Nordman et al. Simulation of toroidal drift mode turbulence driven by temperature gradients and electron trapping. *Nucl. Fusion*, 30(983), 1990.

[23] H. Weisen et al. Shear and collisionality dependences of particle pinch in jet l-mode plasmas. *Plasma Phys. Control. Fusion*, 46(751), 2004.

[24] H. Weisen et al. Isotope dependence of energy, momentum and particle confinement in tokamaks. *J. Plasma Phys.*, 86(905860501), 2020.

[25] ITER Physics Basis Editors et al. Iter physics basis expert groups on confinement and transport and confinement modelling and database. *Nucl. Fusion*, 39(2175), 1999.

[26] J. Citrin et al. Gyrokinetic simulation of collisionless trapped-electron mode turbulence. *Phys. Plasmas*, 12(072309), 2005.

[27] L. Frassinetti et al. Pedestal structure, stability and scalings in jet-ilw: the eurofusion jet-ilw pedestal database. *Nucl. Fusion*, 61(016001), 2021.

[28] M. Fröjdh et al. Impurity effects on η_i mode stability and transport. *Nucl. Fusion*, 32(419), 1992.

[29] M. Maslov et al. Density profile peaking in jet h-mode plasmas: experiments versus linear gyrokinetic predictions. *Nucl. Fusion*, 49(075037), 2009.

[30] M. Valovič et al. On the correlation between density profile and particle flux in h-mode tokamak plasmas and the implication for iter. *Nucl. Fusion*, 47(196), 2007.

[31] P. Mantica et al. Experimental study of the ion critical-gradient length and stiffness level and the impact of rotation in the jet tokamak. *Physical review letters*, 102(175002), 2009.

[32] P. Strand et al. Comparisons of anomalous and neoclassical contributions to core particle transport in tokamak discharges. *31st EPS conferance on Plamsa Phys.*, 28G(P-5.187), 2004.

[33] P.A. Schneider et al. Overview of the isotope effects in the asdex upgrade tokamak. *Plasma Phys. Control. Fusion*, 63(064006), 2022.

[34] R.L. Miller et al. Noncircular, finite aspect ratio, local equilibrium model. *Phys. Plasmas*, 5(973), 1998.

[35] S. Mordijck et al. Collisionality driven turbulent particle transport changes in diii-d h-mode plasmas. *Nucl. Fusion*, 60(066019), 2020.

[36] T. Tala et al. Density peaking in jet - driven by fuelling or transport? *Nucl. Fusion*, 60(066019), 2020.

[37] R.E. Waltz et.al. Gyrolandau fluid models for toroidal geometry. *Physics of Fluids b: Plasma physics*, 4(3138), 1992.

[38] J. P. Freidbert. *Ideal MHD*. Cambridge University Press.

[39] T.S. Hahm and K. Burell. low shear induced fluctuation suppression in finite aspect ratio shaped tokamak plasma. *Phys. Plasmas*, 2(1648), 1995.

[40] H. Hopf. Abbildungsklassenn-dimensionaler mannigfaltigkeiten. *Mathematische Annalen*, 96:209–224, 1927.

[41] F. Jenko and W. Dorland. *Plasma Phys. Contr. Fusion*, 43(12A), 2001.

[42] R. Kubo. The role of zonal flows in the saturation of multi-scale gyrokinetic turbulence. *J. Math. Phys.*, 4(174), 1963.

[43] J. Lawson. Some criteria for a power producing thermonuclear reactor. *Poceedings of the Physical Society. Section B*.

[44] F. Merz. *Gyrokinetic simulation of multiomode plasma turbulence*. PhD thesis, Universität Münster.

[45] P. Strand. *Predictive Simulations of Transport in Tokamaks*. PhD thesis, Chalmers University of Technology.

[46] G. Tardini. *Validation of theory based transport models in tokamak plasmas*. PhD thesis, Technische Universität München.

[47] H. Urano and E. Narita. Review of hydrogen isotope effects on h-mode confinement in jt-60u. *Plasma Phys. Control. Fusion*, 63(084003), 2021.

[48] J. Weiland. *Stability and Transport in Magnetic Confinement Systems*. Springer Series on Atomic, Optical, and Plasma Physics.

[49] J. Wesson. *Tokamaks, Third edition*. Oxford University Press.